catalysts

MDPI

Review

Cold Plasma Techniques for Sustainable Material Synthesis and Climate Change Mitigation: A Review

Nitesh Joshi [1] and Sivachandiran Loganathan [2,*]

[1] School of Chemical Sciences, Goa University, Taleigao Plateau 403206, Goa, India
[2] Department of Civil and Environmental Engineering, University of Nevada, Reno, NV 89557, USA
* Correspondence: sloganathan@unr.edu

Abstract: In recent years, the emission of greenhouse gases (GHGs) has increased significantly, contributing to global warming. Among these GHGs, CH_4, CO_2, and CO are particularly potent contributors. Remediation techniques primarily rely on materials capable of capturing, storing, and converting these gases. Catalytic processes, particularly heterogeneous catalysis, are essential to chemical and petrochemical industries as well as environmental remediation. Due to the growing demand for catalysts, efforts are being made to reduce energy consumption and make technologies more environmentally friendly. Green chemistry emphasizes minimizing the use of hazardous reactants and harmful solvents in chemical processes. Achieving these principles should be paired with processes that reduce time and costs in catalyst preparation while improving their efficiency. Non-thermal plasma (NTP) has been widely used for the preparation of supported metal catalysts. NTP has attracted significant attention for its ability to improve the physicochemical properties of catalysts, enhancing process efficiency through low-temperature operation and shorter processing times. NTP has been applied to various catalyst synthesis techniques, including reduction, oxidation, metal oxide doping, surface etching, coating, alloy formation, surface treatment, and surface cleaning. Plasma-prepared transition-metal catalysts offer advantages over conventionally prepared catalysts due to their unique material properties. These properties enhance catalytic activity by lowering the activation energy barrier, improving stability, and increasing conversion and selectivity compared to untreated samples. This review demonstrates how plasma activation modifies material properties and, based on extensive literature, illustrates its potential to combat climate change by converting CO_2, CH_4, CO, and other gases, showcasing the benefits of plasma-treated materials and catalysts. A succinct introduction to this review outlines the advantages of plasma-based synthesis and modification over traditional synthesis techniques. The introduction also highlights the various types of plasma and their physical characteristics across different factors. Additionally, this review addresses methods by which materials are synthesized and modified using plasma. The latter section of this review discusses the use of non-thermal plasma for greenhouse gas mitigation, covering applications such as the dry reforming of CH_4, CO and CH_4 oxidation, CO_2 reduction, and other uses of plasma-modified catalysts.

Keywords: cold plasma; catalyst synthesis; surface modification; greenhouse gas remediation; environmental application

Citation: Joshi, N.; Loganathan, S. Cold Plasma Techniques for Sustainable Material Synthesis and Climate Change Mitigation: A Review. *Catalysts* **2024**, *14*, 802. https://doi.org/10.3390/catal14110802

Academic Editor: Sergio Nogales Delgado

Received: 7 October 2024
Revised: 4 November 2024
Accepted: 6 November 2024
Published: 8 November 2024

1. Introduction

The environment and its components are severely polluted, and climate change has become a serious concern that requires urgent action. Climate change is occurring in real-time, driven by the emission of greenhouse gases (GHGs) into the atmosphere, leading to a global increase in temperature known as global warming. Among the various GHGs, CO_2, CH_4, and CO are particularly significant due to their high global warming potential.

To address this modern-day problem, many technologies have been developed, with catalysis emerging as a key solution. According to IUPAC nomenclature, catalysis is the

process of increasing the rate of a chemical reaction by adding a catalyst [1]. Catalysts are now employed across diverse fields, including industrial, environmental, fuel, and energy sectors. Given the wide range of applications and the complexity of processes involving catalysts, there is a need to design and develop catalysts tailored to specific applications. Catalytic processes are heavily influenced by surface morphology and chemical composition.

Several techniques are available for catalyst synthesis, ranging from simple thermal treatment to more complex methods [2]. The thermal treatment, i.e., calcination, depends on the operating temperature. A high calcination temperature can cause unwanted catalyst morphologies, such as sintering, agglomeration, and reduced activity, due to a decreased surface area and the undesirable oxidation of active metal centers [3]. Therefore, researchers are exploring new techniques that can control size, morphology, and composition under milder conditions compared to conventional methods. Additionally, these processes should be straightforward and less complex to ensure cost-effectiveness and user-friendliness.

Conventional materials can be treated during or after "classical" synthesis, often resulting in new materials with distinct properties. Remarkably, these modified materials have shown advantages over unmodified ones. Plasma treatment differs from the conventional synthesis method, as reported in Table 1. Plasma treatment is ideally a solvent-free and ligand-free approach, reducing the risk of contaminants. In conventional synthesis, nanoparticles are typically formed from a liquid state, whereas plasma treatment can produce crystalline forms along with the liquid state. The size and distribution of nanoparticles in plasma-treated samples range from 2 to 10 nm, achieving uniformity that is challenging to attain in conventional synthesis due to the thermal sintering effect. Plasma treatment also prevents particle agglomeration and offers a turnkey process that is easy to switch on and off. The plasma operating procedure is easily tuneable and operates at low operating conditions. In addition, the nanoparticle growth is irreversible, which infers that particle growth is unaffected due to external parameters like heat. The plasma treatment time is very short in comparison to conventional synthesis, which can take several hours.

Table 1. Difference between conventional and plasma treatment for catalyst synthesis/modification.

	Conventional	**Plasma**
Solvent- and Ligand-Free Approach	×	√
Purity	Low (Material Needs to be Purified)	High Purity
Form of Synthesis	In Aqueous-Phase Synthesis	Crystalline-Form Synthesis Possible
Characteristics of Material Synthesized		
Size	Difficult to Synthesize < 10 nm	2–10 nm
Control Over Agglomeration	×	√
Possibility of Tuning Sites on Catalyst Surface	×	√
Possibility to Stop Process Intermediate Stage?	×	√
Operating Temperature	High	Low
Nanoparticle Growth	Reversible	Irreversible
Treatment Duration	Long	Short

Plasma is a cocktail of reactive species, which makes it different from a normal gas mixture. The composition of plasma is quite complex and includes neutral molecules, positively charged ions, electrons, radicals, and other components [4,5]. Plasma is classified as thermal or non-thermal based on the gas temperature. In thermal plasmas, a local thermodynamic equilibrium (LTE) between all species is attained. Moreover, the bulk gas temperature is raised to several thousands of Kelvins. In NTPs, the species (electrons, ions, neutral molecules, etc.) have a different temperature in a localized area and, thus, distort from equilibrium and are referred to as non-equilibrium plasmas or cold plasma. Typically, in NTPs, the temperature of neutral species is close to ambient temperature and the electrons' temperature is higher than 10,000 K, called hot electrons.

The hot electrons collide with gas molecules to effectively dissociate and, thus, ionized gaseous species are formed. These radicals and ions react exothermically on the nanoparticle surfaces. This leads to the heating of the nanoparticles to a temperature of hundreds of Kelvin above the neutral gas temperature, and this mechanism prevails in the NTP-assisted catalyst synthesis of nanocrystals.

The energy involved in thermal plasmas is higher than that for thermal calcination. Therefore, as shown in Figure 1, they are widely used in energy-intensive processes like catalyst synthesis, metal oxide deposition, alloying, etching, and other applications. It is well known that thermal heating is nonselective as all degrees of freedom are equally activated. In gliding arc plasmas, the gas temperature would reach about 3000 K and is used in material oxidation, reduction, and doping (ORD) applications. NTPs have the lowest gas temperature and can be used for catalyst synthesis as they can initiate the reactions at mild conditions and within a short treatment time. Thus, for temperature-sensitive precursors and catalysts, using non-thermal plasma has an added advantage over other techniques.

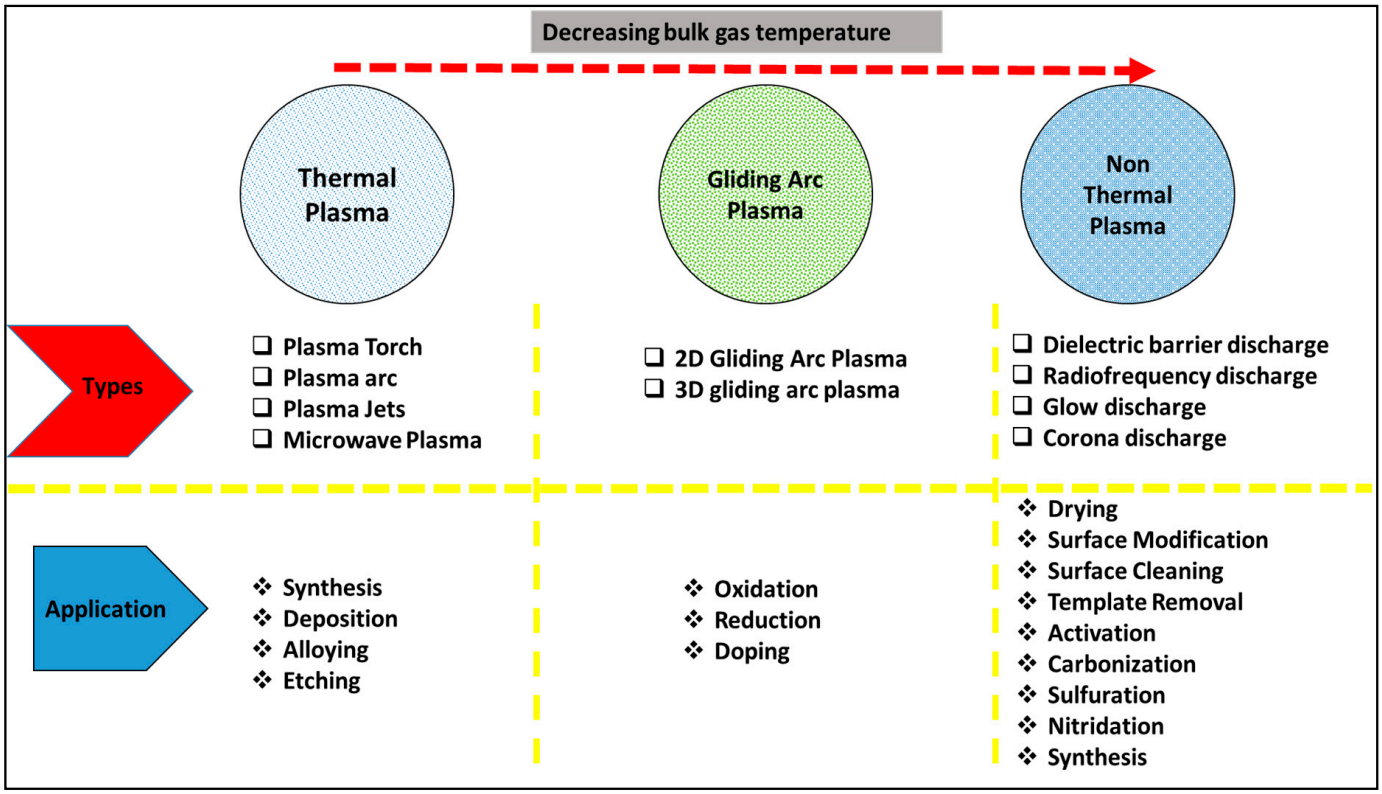

Figure 1. Different types of plasmas and their applications in material and catalyst synthesis.

Conventionally, the chemical vapor deposition technique (CVD) is employed for the deposition of thin films. However, the organic and/or metalorganic precursors have to be vaporized to be introduced into the reactor, but the precursors with lower vapor pressures inflict problems on operations. The above-stated issues can be resolved using an innovative plasma-enhanced chemical vapor deposition (PECVD) technique. This is where plasma is applied to deposit a thin film of a particular material on any support. Apart from organic and metal-organic precursors, metal precursors have also been used for film deposition. A significant advantage of PECVD is that a catalyst can be directly deposited on the metal rod or graphite rod using neither a precursor nor a capping agent. The simplicity and high reproducibility of the direct vaporization and deposition of metallic materials onto oxide supports are the other added advantages of plasma deposition.

This review focuses on the application of various NTPs for material and/or catalyst synthesis, surface modification, and catalyst reduction. Comprehensive literature studies are presented to demonstrate the effectiveness of plasma in catalytic activities for remediation from climate change by mitigating GHGs. The aim is to demonstrate the superiority of plasma-aided catalyst synthesis/modifications over conventional catalysts. Indeed, catalyst synthesis using cold plasmas and their environmental applications are emphasized.

Non-thermal plasma (NTP) is emerging as a transformative technology with diverse applications across several critical sectors. In environmental protection, NTP is increasingly recognized for its effectiveness in pollution control, particularly for removing harmful substances like nitrogen oxides (NOx) and volatile organic compounds (VOCs). Recent studies have highlighted its ability to decompose NOx emissions from diesel engines and various industrial sources, with enhanced efficiency achieved through integration with catalytic processes [6,7]. This capability positions NTP as a promising solution for meeting stringent environmental regulations. Additionally, NTP shows potential in wastewater treatment and air purification, where its generation of reactive species facilitates the breakdown of complex organic pollutants, contributing to cleaner industrial practices.

In the medical field, NTP is gaining traction due to its unique properties that enable non-invasive treatments. Bibliometric analyses indicate growing interest in its therapeutic applications, such as wound healing, where NTP promotes cell proliferation and tissue regeneration while effectively inactivating bacteria, including antibiotic-resistant strains. Research further suggests that NTP can induce apoptosis in cancer cells through the production of reactive oxygen and nitrogen species, presenting it as a potential adjunct therapy in oncology. Its antimicrobial properties are also harnessed for sterilizing medical instruments and surfaces, significantly enhancing safety in healthcare settings [8].

The food industry is also exploring NTP as an innovative method for the microbial decontamination of fruits, vegetables, and meat products—especially beneficial for items sensitive to heat or chemical treatments. Recent advancements demonstrate that NTP can effectively reduce microbial loads while preserving food quality. Research is also examining its role in enzyme inactivation and pesticide reduction, further bolstering food safety [9].

Furthermore, NTP is making significant strides in industrial catalysis, enabling chemical reactions at lower temperatures than with traditional methods, which not only saves energy but also minimizes the thermal degradation of sensitive reactants. Developments such as packed bed plasma-catalytic reactors have shown improvements in reaction rates and product yields, indicating that the combination of NTP with catalysts is revolutionizing various chemical manufacturing processes [10]. The applications of non-thermal plasma are rapidly expanding across multiple industries, fueled by ongoing research and technological advancements. Its ability to operate at low temperatures while generating reactive species makes NTP a versatile and powerful tool for addressing contemporary challenges in environmental protection, healthcare, food safety, and industrial processing. As research evolves, the promise of NTP for broader applications and improved efficiencies in these critical areas remains bright and exciting.

2. NTP and the Types Used for Material Synthesis/Modification

As shown in Figure 1, NTPs are distinguished into various types, discussed below.

Radiofrequency (RF) Discharge: RF discharges generally operate at very high frequencies, in the range of several MHz, and at low pressure. RF discharge is used industrially and in the laboratory to generate plasma sources for optical emission spectroscopy and plasma chemical investigations. The best example of RF plasma is inductively coupled plasma (ICP), which operates at 2–60 MHz. RF plasma has also been used for etching metal surfaces when operated at low pressures. RF plasma is generated without electrodes and the plasma is generated by an inductive effect due to the very high frequencies. Figure 2 depicts a schematic of RF plasma.

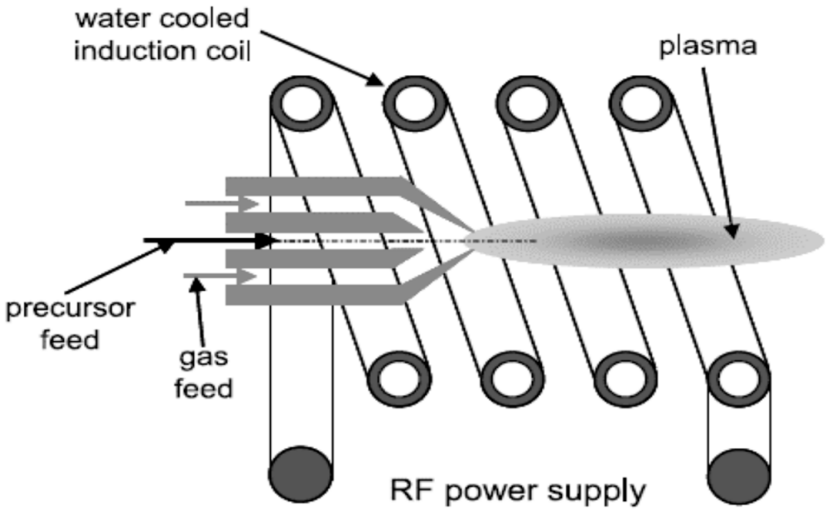

Figure 2. Schematic of RF plasma (inductively coupled plasma) employed for powder synthesis. Reproduced with permission from [11].

Glow Discharge (GD): GD plasma can be termed as a partially ionized low-pressure gas in a quasi-neutral state sustained by the presence of energetic electrons. The character of such plasmas is a consequence of the mass difference between the electrons and ions. Due to this mass difference, energy is transferred more rapidly to the electrons than to the ions. These energetic electrons then accumulate sufficient energy to have a high probability of causing ionization and excitation events when colliding with heavier particles. The generation of these particles and their interactions with surfaces and growing films are the most important reasons why GD plasmas have been widely used in materials science [12]. To have a discharge, flat electrodes encapsulated in the tube are employed. Figure 3 depicts a schematic representation of GD plasma. As stated previously, GD is a type of NTP, where the glow is generally created by the excitation of neutral atoms and molecules. If the GD operates at low pressures, a vacuum system is usually connected to the reactor. Upon connecting the vacuum system, the energy loss resultant from intermolecular collisions is reduced and, thus, plasma is ignited using DC voltages. However, if one tries to ignite GD under atmospheric conditions, one needs to apply high AC voltages of the order of several kV (kilo volts). Commonly, DC (direct current) voltage ignites plasmas in a glow discharge. Since these plasmas operate at low pressure and limited mass flow, their use in industry is undesirable. However, neon signboards and fluorescent tubes are the practical applications of glow discharges. The physical operating parameters of GD are given in Table 2.

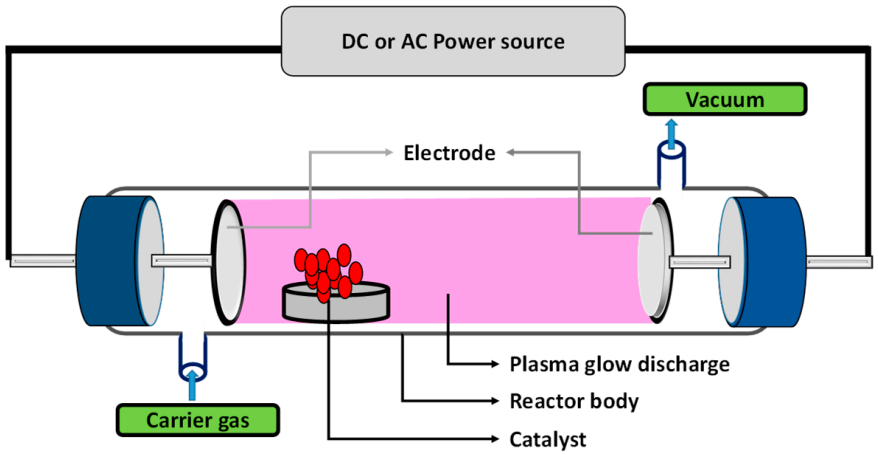

Figure 3. Schematic of GD for material synthesis.

Table 2. The parameters of various non-thermal plasma gas discharges, adapted from [13].

	Glow Discharge	Corona	DBD
	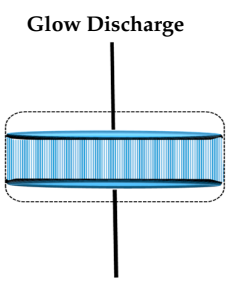	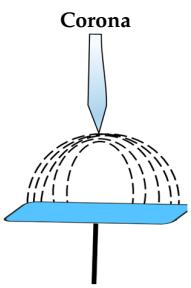	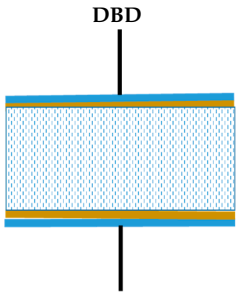
Pressure (kPa)	<1	100	100
Electric Field (kV/cm^2)	0.01	0.5–10 variable	0.1–100
Reduced Field (Td)	50	2–200	1–500
Electron Energy (eV)	0.2–2	5	1–10
Electron Density (cm^{-3})	10^8–10^{11}	10^{-3}	10^{14}
Degree of Ionisation	10^{-6}–10^{-5}	Nil	10^{-4}

Corona Discharge (CD): CD is inhomogeneous and can be initiated at atmospheric pressure in *pin-to-plate and/or wire-to-plate* electrodes. In CD, electrical discharges between two electrodes occur in the gas phase when the induced electric field exceeds the breakdown voltage required to ionize or excite the gas. However, the applied voltage should be insufficient to cause a spark. It should be noted that at atmospheric pressure, corona discharge produces several active species in less than tens of milliseconds. It has been widely used in industries including electrophotography, printing, textile processing, and in-powder coating. Nevertheless, due to their inherent non-uniformity, it has limited applications for homogeneous treatments and coating depositions.

Dielectric Barrier Discharge (DBD): In DBD, one or both electrodes are covered by a dielectric material like ceramics, glass, quartz, and catalysts. In a two-electrode setup, i.e., in CD, when a sufficient electric field is accumulated on the electrodes, discharge is initiated. However, in DBD, the dielectric material accumulates charges, and these charges form an opposite electric field that opposes the electric field generated on the electrode. This restricts the current flow through the reactor from one electrode to another; the process occurs in a sub-microsecond regime which gives microdischarges. A schematic of the various types of DBD reactors is reported in Figure 4.

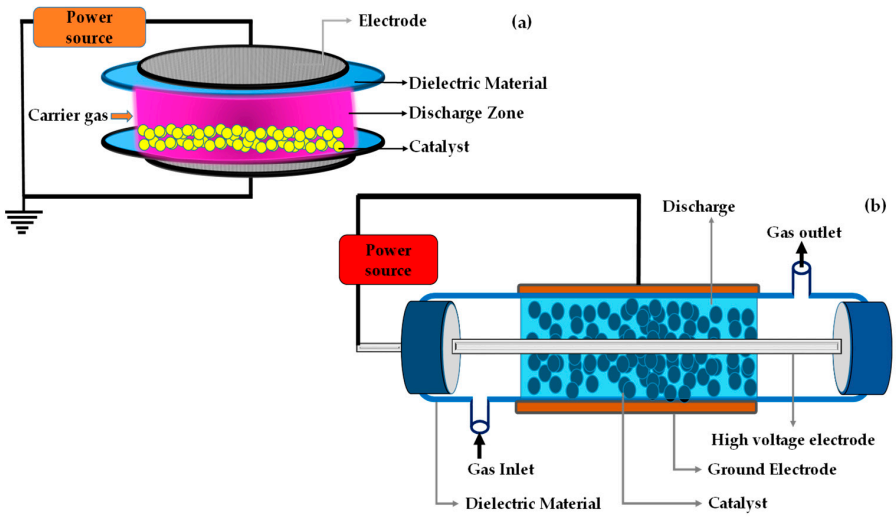

Figure 4. DBD setup scheme: (**a**) plate–to–plate DBD reactor separated by quartz discs and (**b**) coaxial DBD reactor.

Plasmas can be employed for catalyst synthesis in two distinct ways:

(1) They can be used during the synthesis of the catalyst or (2) they can be applied after catalyst synthesis to bring surface modifications to the catalyst.

It should be noted that it is still unclear how plasma and its physical properties influence material synthesis/modification. However, as can be seen from Table 2, DBD plasma seems to be the most energetic, with an electron energy of about 1–10 eV in ambient conditions. The subsequent section of this review will illustrate the impact of plasma on the synthesis/modification of materials and its application for greenhouse gas (GHG) mitigation. In recent years, significant attention has been focused on utilizing plasma for the synthesis of catalysts, as exemplified in Figure 5. The reason is that plasma treatment leads to the generation of such changes that are difficult to achieve in normal circumstances. As can be seen from Figure 5a, in this decade, from 2010 to 2024, a lot of effort has been driven towards the employment of NTPs for material treatment and a variety of other applications. Figure 5b depicts the contribution of various types of non-thermal plasma used for catalyst synthesis. Currently, more effort is being driven towards the synthesis of catalysts using plasma generated at atmospheric pressure, namely, CD and DBD. To the best of our knowledge, to date, several review articles [14–26] and book chapters [27,28] have been published on the synthesis/modification of materials for environmental applications. However, to date, comprehensive literature reviews on the use of NTPs for material modification/synthesis to combat climate change are unavailable. Thus, this review deals with the topic of GHG mitigation with plasma-activated catalysts.

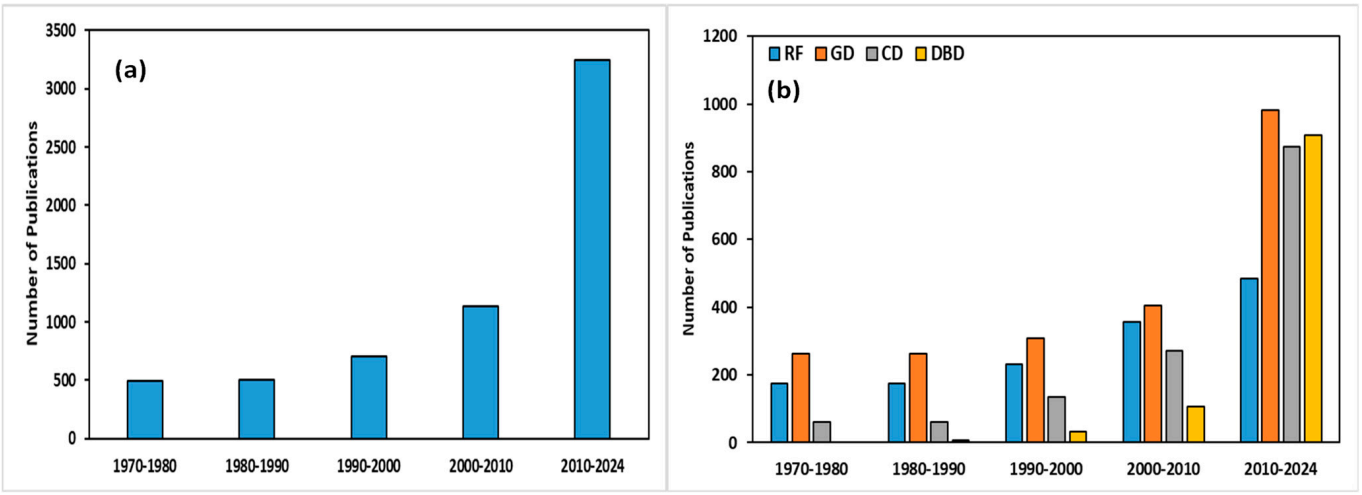

Figure 5. (**a**) Number of publications in the past 5 decades that deal with the use of non-thermal plasma for catalyst synthesis. (**b**) Number of publications on different types of non-thermal plasma employed for catalyst synthesis. Source: ScienceDirect. Keyword: catalyst preparation using NTP.

3. Mechanism of Nanoparticle Formation, the Modification of Surfaces, and the Improvement in Dispersion

In NTPs, the electrons are the main species and play an important role in modifying materials with plasmas by direct surface reactions. Due to their extremely low mass, the electrons have a minimal impact on the material. This results in a difference in the collisional frequency of electrons that is 2–3 times higher than that for ions [29]. The energetic electrons with sufficient kinetic energy ionize and excite the heavier molecule when it collides; these ions may internally change the material surface. Thus, the majority of plasma energy is absorbed by electrons and not by ions. Table 3 presents a comparative analysis of the energy and kinetic velocities exhibited by ions and electrons. Noteworthy disparities in both energy and velocity are apparent when comparing electrons and ions.

When a material is introduced to plasma, it acquires a negative charge due to the high kinetic velocity of electrons. These negative changes attract positively charged ions, resulting in effective collisions. The effectiveness of plasma in a specific process, whether

synthesis or modification, is contingent upon the energy distribution of electrons within plasma. This energy distribution adheres to Maxwellian distribution, and only the hot electrons with abundant energy are capable of colliding with the material of significance.

Table 3. Energy and mean kinetic velocity of species in non-thermal plasma, adapted from [18].

Species	Energy		Mean Kinetic Velocity (m/s)
	Electron Volts (eV)	Kelvin (K)	
Electrons (e^-)	1–5	11,000–55,000	6.6×10^5–1.5×10^6
Ar^+	0.025–0.1	300–1200	~400–800
He^+	0.025–0.1	300–1200	~1200–2400

As seen from Figure 6, the occurrence of nanoparticles from a solution/substrate hinges on the charging process. The formation of nanoparticles commences with the seeding/nucleation phase, succeeded by the aggregation of nanoparticles to form crystallites, and then further growth. The nuclei or seeds arise from the accumulation of charges, be they neutral or singly negative. The particles emerging from the nucleation stage are initially diminutive and uniformly negatively charged. Larger particles develop through the interplay of neutral nuclei particles and clusters. This progression persists until the particles have grown larger than the parent. At this juncture, all particles are negatively charged, and agglomeration halts.

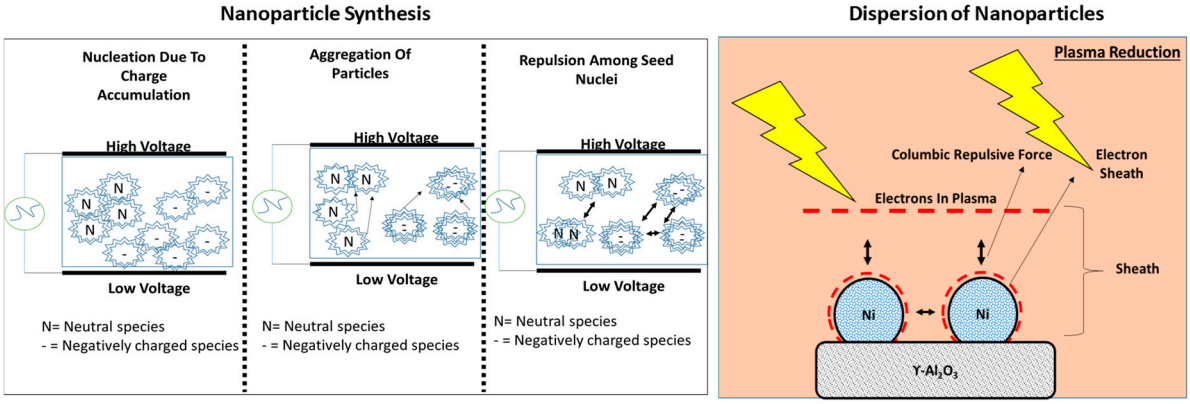

Figure 6. Mechanism of nanoparticles forging from medium and the dispersion of nanoparticles.

The negative charge sheath is created around particles, and the particles carry one or two elementary charges per nanometer of their radius. For the uniform dispersion of nanoparticles, columbic repulsion is important. It could be that upon exposure to a plasma catalyst, particles and/or crystallites act as an electron sink. The plasma application leads to the generation of a space-charge sheath in the vicinity of the catalytic surface, and the material surface is charged negatively. Hence, there also exists a repulsive Coulombic force between the two particles that possess the same negative charge; this induces the separation of one catalyst particle from the other and thus leads to better dispersion and a smaller particle size. Figure 6 gives a pictorial representation of a plausible mechanism that may operate in plasma and lead to enhanced metal dispersion [17].

4. Plasma-Modified Catalyst for the Mitigation of GHGs

The mitigation of GHGs, namely, CH_4, CO_2, CO, and others, is demonstrated in the upcoming sections.

4.1. Dry CH_4 Reforming Using a Plasma-Modified Catalyst

Plasma treatment has been reported to enhance metal–support interaction. For instance, authors employed RF plasma treatment on a Ni-Pt bimetallic/MgAlO catalyst for

120 min, resulting in a shift in the Ni^{+2} reduction peak by 90 °C in comparison to the untreated sample. This shift indicated improved metal–support interactions. Additionally, the dispersion of Ni^0 on the support was significantly higher in the plasma-treated sample, which was then used for the dry reforming of CH_4. The plasma-treated sample achieved CH_4 and CO_2 conversion of 31.7 and 32.8%, respectively, while the untreated sample exhibited only 28.8 and 29.0% conversion at an operating temperature of 550 °C HAO [30].

In another study, plasma treatment demonstrated superior catalyst stability for the CO_2 reforming of CH_4 [31]. The authors treated a NiMgSBA-15 catalyst with RF plasma (13.56 MHz frequency, 100 V, anodic current of 100 mA, 2 h treatment, and gas pressure of 50 Pa). This plasma treatment minimized carbon deposition on the active Ni sites due to improved dispersion, and the increased Lewis basic sites enhanced CO_2 adsorption and metal–support interactions. As a result, the plasma-treated sample showed higher CH_4 and CO_2 conversions than the calcined sample under the same conditions. Furthermore, the plasma-treated catalyst exhibited prolonged catalytic stability and high CO and H_2 selectivity over 100 h, while the thermally calcined sample lost activity after only 10 h of reaction. Through extensive pre- and post-treatment catalyst characterization, the authors attributed the benefits of plasma-treated catalysts to (i) stronger basicity, which enhanced CO_2 adsorption, and (ii) reduced Ni particle size, leading to better Ni–support interactions.

RF plasma treatment has been shown to promote the migration of Ni^{+2} species from the bulk to the surface of a Ni-Pt bimetallic/MgAlO catalyst after 120 min of treatment. This could be due to the high potential difference applied, causing Ni^{+2} migration to the surface and resulting in higher conversion rates compared to the untreated sample when used for CH_4 dry reforming [30].

In another study, a Ni/Al_2O_3-ZrO_2 catalyst was synthesized by the wet impregnation method and subsequently treated with DC-GD plasma at 1 kV and 100–200 Pa of pressure for 15 min. After plasma treatment, the sample was calcined at 600 °C for 5 h under airflow. Testing the catalyst for the CO_2 reforming of CH_4 showed enhanced CO and H_2 production at lower temperatures than the calcined catalyst. This improvement was attributed to the highly dispersed NiO nanoparticles, increased surface area, and strong active phase interaction with the Al_2O_3 support. Similarly, a coke-resistant Ni/SiO_2 catalyst synthesized using GD plasma treatment demonstrated increased Ni particle dispersion and stronger SiO_2 interaction. The plasma-treated Ni/SiO_2 catalyst showed commendable activity compared to a Ni/SiO_2 catalyst calcined at 500 °C for 4 h. The plasma-treated sample achieved 100% conversion of CH_4 and CO_2, compared to 78 and 75% for the thermally calcined catalyst at a reaction temperature of 850 °C [32].

Researchers have increasingly focused on the reduction of catalysts under mild conditions, utilizing GD plasma–catalyst interactions for the CO_2 reforming of CH_4. In one study, a coke-resistant Ni/SiO_2 catalyst prepared with GD plasma exhibited superior performance to a catalyst synthesized thermally at 500 °C. The GD plasma treatment improved metal–support interactions, resulting in a highly dispersed NiO layer on the surface. The study confirmed that catalysts prepared under milder plasma discharge conditions can outperform those synthesized at high temperatures [33].

Another investigation explored the effect of GD plasma on a Ni/Al_2O_3 catalyst preparation for the CO_2 reforming of CH_4. Plasma treatment was conducted at room temperature under an Ar atmosphere (100–200 Pa) for 15 min; this was repeated three times and followed by calcination at 600 °C for 6 h. XRD analysis revealed the absence of Ni, NiO, and $NiAl_2O_4$ peaks in the plasma-treated sample, even with 9% Ni loading, suggesting a very small particle size and high surface dispersion. Further examination confirmed that the Ni particle size remained below 5 nm, even after 10 h of catalytic reaction at 550 °C, highlighting the stability and anti-sintering properties of the plasma-treated catalyst (Figure 7). The GD plasma treatment induced significant surface changes, enhancing catalytic activity and reducing carbonaceous species (Cγ) deposition [34].

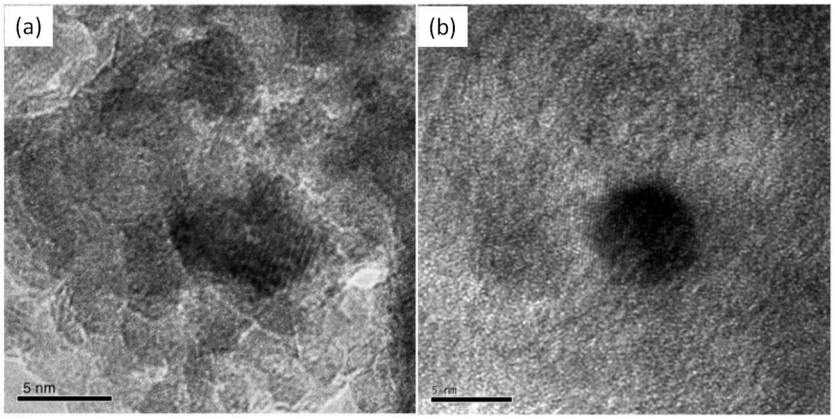

Figure 7. TEM image of Ni (9%)/Al_2O_3 catalyst: (**a**) before reforming reaction and (**b**) after reforming reaction at 550 °C for 10 h. Reproduced with permission from [34].

In another study, Zhao et al. [35] studied the effect of Ar-GD plasma (100–200 Pa, 900 V) on Ir (1 wt%)/γ-Al_2O_3 catalyst surface modification and tested the catalyst for the CO_2 reforming of CH_4. They evidenced that the plasma-treated catalyst showed higher conversion compared to the conventionally reduced catalyst under similar operating conditions. The CO chemisorption study revealed that the plasma-treated sample possessed very high dispersion (about 84%) and a smaller particle size (<2 nm) compared with the H_2-reduced sample at high temperatures. However, the authors did not discuss how or why the Ar-GD plasma improved the Ir particle dispersion and controlled the particle size. Apart from the uniform dispersion and generation of smaller particle sizes of active metal atoms, Liu et al. [36] reported that the surface acidity of a catalyst could also be increased by GD plasma treatment. Pd/NaZSM-5 and Pd/HZSM-5 catalysts were treated by plasma and utilized for syngas production from CH_4. It was demonstrated that the plasma-treated sample exhibited enhanced conversion and higher syngas selectivity, as well as less carbon deposition on the surface.

Besides applying DBD plasma for catalyst synthesis, many articles focus on catalyst reduction using plasma. For instance, Karuppiah and Mok [37] used a DBD reactor to reduce Ni/γ-Al_2O_3 and CeO_2-Ni/γ-Al_2O_3 catalysts. The plasma reduction was carried out with 11–12.5 kV of applied voltage, 1 kHz of frequency, 100 W of input power, and a plasma treatment time of 4 h. The catalyst activity was tested for propene reforming with CO_2. The plasma-reduced catalyst showed enhanced conversion in comparison to the thermally reduced catalyst. Additionally, the plasma-treated sample gave a higher H_2/CO ratio in contrast to the thermally treated samples. The superior behavior of the plasma-reduced sample was due to the uniform distribution of active metal on the support. The tuneable oxidation states of the metal oxide catalyst could be achieved by varying the plasma input power. The authors reduced 1 g of $Ni(NO_3)_2$/γ-Al_2O_3 through a 20 min plasma treatment with a fixed 40 kV of applied potential, but varied the frequency between 10 and 40 kHz. The authors showed that the plasma input power had a strong dependence on the degree of reduction. For instance, at a power below 40 W (at 270 °C), the $Ni(NO_3)_2$ was decomposed to NiO; however, at a higher power, the $Ni(NO_3)_2$ was reduced to Ni^0. The synthesized catalyst was used for the CO_2 reforming of CH_4. Moreover, it was reported that the plasma-treated catalysts exhibited better activity, stability, and anti-carbon deposit performances, which were mainly ascribed to a smaller Ni particle size and more basic sites on the catalyst surface [38].

The removal of carbonates during the synthesis of Ni/MgO was reported by Hua et al. [39]. The authors used DBD plasma to treat co-precipitated $NiCO_3$-$MgCO_3$ and Ni/MgO catalysts for the CO_2 reforming of CH_4. The catalyst prepared via plasma had a higher specific surface area and smaller particle size, as seen in Figure 8a,b, and the CH_4 and CO_2 conversion rates were increased by more than 20% in comparison to the untreated sample, which was coherent with the particle size of Ni.

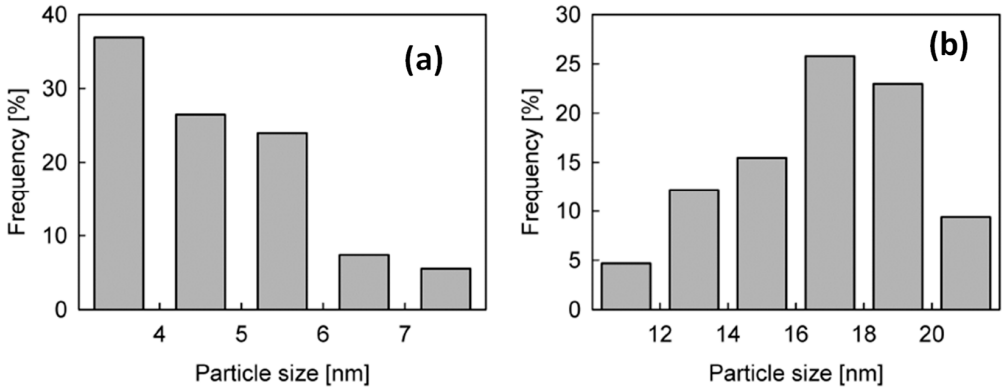

Figure 8. Ni particle size distributions in (**a**) plasma-treated and (**b**) conventional treatment of Ni/MgO catalysts. Reprinted with permission from [39].

$Ni/Y_2Zr_2O_7$ was synthesized using a $Ni(NO_3)_3$ (99.9%) solution that was impregnated with $Y_2Zr_2O_7$. The impregnated sample was divided into four parts: one part was thermally calcined at 800 °C, while the remaining parts were treated using DBD plasma in air, Ar, and a mixture of H_2/Ar (DBD plasma operating conditions: 100 V and 1 A) [40]. The CO_2 reforming of CH_4 was carried out using the catalyst, and the results are presented in Figure 9. Compared to the untreated sample, the plasma-treated sample exhibited significantly higher conversion rates. This enhancement was attributed to the more homogenous distribution of Ni^0 on the support. Furthermore, varying the plasma treatment gas revealed that the H_2/Ar mixture resulted in significantly higher conversion compared to Ar or air alone. The authors also observed a corresponding decrease in Ni particle size following the same trend. However, the authors neither explained nor hypothesized the underlying reasons for this observation. It can be speculated that the higher reduction capacity of the H_2/Ar mixture compared to Ar could account for the improved performance.

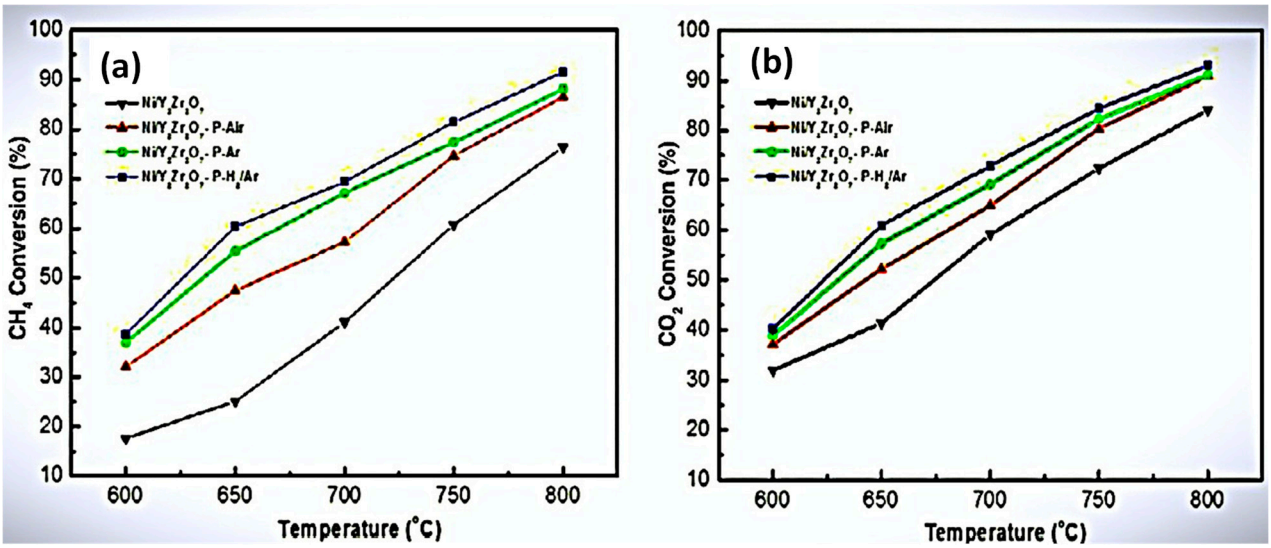

Figure 9. Reaction performance of $Ni/Y_2Zr_2O_7$ untreated and treated catalysts: (**a**) CH_4 conversion and (**b**) CO_2 conversion. Reproduced with permission from [40]. P = plasma treatment, Ar = argon atmosphere, H_2/Ar = mixture of H_2 and Ar.

Table 4 summarizes the literature studies on different types of catalysts, plasma and thermal modification conditions, and the performance of modified catalysts for the dry reforming of CH_4. Additionally, the advantages of plasma treatment over thermal treatment for catalyst properties are highlighted.

Table 4. Comparative table for operating conditions, performance, and advantages of plasma over thermal modification techniques for CH_4 dry reforming.

Catalyst	Catalyst Treatment Conditions		Conversion and Yield		Advantage of Plasma-Treated Catalyst over Thermally Treated Materials	References
	Plasma	Thermal	Plasma-Treated	Thermally Treated		
Ni-Pt bimetallic/MgAlO	**RF plasma** (voltage 100 V, frequency 13.56 MHz, and initial gas pressure 50 Pa for nitrogen plasma for 60 min and then for hydrogen for another 60 min at ambient temperatures)	Calcined at 500 °C for 8 h, air flow	CH_4: 31.7%, CO_2: 32.8%	CH_4: 28.8%, CO_2: 29.0%	Enhanced metal–support interaction, better dispersion	[30]
NiMgSBA-15	**RF plasma** (voltage 100 V, frequency 13.56 MHz, current 100 mA, and initial gas pressure 50 Pa for N_2 Plasma for 120 min)	Calcined at 550 °C for 6 h, air flow	CH_4: <85%, CO_2: 85%	CH_4: >85%, CO_2: 80%	Superior performance due to better Ni dispersion, lack of carbon deposition, increased basic sites	[31]
Ni/Al_2O_3-ZrO_2	**DC-GD** (voltage 1 kV and initial gas pressure 100–200 Pa for Ar plasma for 15 min at room temperature, then calcined at 600 °C in air)	Calcined at 600 °C for 5 h, airflow	CH_4: <90%, CO_2: 80%	CH_4: ~80%, CO_2: <95%	Highly dispersed NiO, strong interaction with support	[32]
Ni/SiO_2	**DC-GD** (voltage 900 V and initial gas pressure of Ar plasma 100 Pa at room temperature and then thermally calcined at 650 °C for 4 h)	Calcined at 650 °C for 4 h	<65% CO_2 and CH_4 conversion	>60% CO_2 and CH_4 conversion	Active metal surface area increased by 1.6 times, 1.58-fold improved metal dispersion, 1.6-fold lowering in crystallite size leading to better interaction and activity compared to calcined sample	[33]
Ni/SiO_2	**DC-GD** plasma at room temperature (voltage 100 V and initial pressure of N_2 plasma 200 Pa for 15 min, then calcined at 600 °C for 6 h)	Calcined at 600 °C for 6 h in air	-	-	Significant improvement in NiO dispersion, no carbon deposition	[34]
Ir (1 wt%)/α-Al_2O_3	**GD plasma** (voltage 900 V and initial pressure of Ar plasma 100–200 Pa)	Calcined at 500 °C for 4 h in air	CH_4: <65%, CO_2: 75%	CH_4: >35%, CO_2: >40%	High dispersion (84%), smaller particle size (<2 nm)	[35]
Pd/NaZSM-5	**GD Plasma** (conditions not specified) and calcined at 673 °C in air	Calcined at 673 °C in air	100% CH_4 conversion at 450 °C	50% CH_4 conversion at 450 °C	Less carbon deposition, increased surface acidity by 21%, 4.4% improved Pd dispersion, 3.4% lower particle diameter, 15.2% improved surface area of Pt (m^2/g metal)	[36]
Ni/γ-Al_2O_3	**DBD plasma** (11–12.5 kV, 1 kHz, 100 W, and 4 h in Ar/H_2 (20%) atmosphere, flow rate 100 mL/min)	Thermal reduction at 500 °C for 6 h in H_2 atmosphere	C_3H_8: 40% CO_2 produced: 30%	C_3H_8: >30% CO_2 produced: >30%	Uniform distribution of active metal, better activity	[37]
Ni/γ-Al_2O_3	**DBD plasma** (maximum voltage of 40 kV and adjustable frequency between 10 and 40 kHz to treat the sample for 20 min)	Thermal reduction at 700 °C for 2 h with 20% H_2/N_2 atmosphere and flow rate of 250 mL/min	CH_4: <40%, CO_2: 45%	CH_4: >30%, CO_2: >38%	More homogeneous distribution, smaller Ni particle size	[38]
Ni/MgO	**DBD plasma** (4 kV, frequency of 18.45 kHz, And 26.5 W power for H_2 plasma with a flow rate of 60 mL/min for 60 min)	Calcined at 700 °C in air for 4 h	CH_4: <45%, CO_2: <55%	CH_4: >30%, CO_2: 20%	6-fold lowering in particle size, higher specific surface area, better activity and stability	[39]
$Ni/Y_2Zr_2O_7$	**DBD plasma** (current applied to electrode of 100 V and 1 A in H_2/Ar for 30 min)	Calcined at 550 °C for 4 h in air	CH_4: <90%, CO_2: <90%	CH_4: >75%, CO_2: >80%	2-fold lowering in particle size and dispersion of metal over support, higher metallic Ni active surface areas achieved, elevated coke resistance	[40]

4.2. Plasma-Treated/Modified Catalyst for Hydrogenation Reactions

GD plasma was utilized to synthesize an Fe-Cu/SiO_2 catalyst for CO hydrogenation to alcohol. The plasma was generated at a frequency of 13.56 MHz, with a potential of 100 V and an anodic current of 50 mA. A 45 min plasma treatment resulted in a 1.6-fold increase in CO conversion and enhanced selectivity towards higher hydrocarbons compared to the untreated catalyst. The authors attributed this improvement to the synergic interaction between iron and copper, which was enhanced by the plasma technique. Plasma application also doubled the Cu/Si surface ratio in the treated sample compared to the conventional catalyst. Additionally, the plasma treatment led to a threefold reduction in crystallite size.

Notably, thermal calcination after plasma treatment did not diminish CO conversion. In comparison to the untreated sample, which achieved 36% CO_2 conversion, the plasma-treated catalyst showed a twofold increase in conversion [41].

Chen et al. [42] synthesized a Pd (0.15 wt%)/α-Al_2O_3 catalyst for the selective hydrogenation of acetylene (C_2H_2) to ethylene (C_2H_4), using H_2 gas as a reducing medium in plasma GD. The plasma was operated for 85 min at a frequency of 13.56 MHz with 100 V and a pressure range of 2 to 200 Pa. At a temperature below 50 °C, the GD-treated sample achieved complete C_2H_2 conversion with 71.3% C_2H_4 selectivity. Contrarily, the thermally treated sample, reduced in H_2 flow at 450 °C, showed no activity under the same operating conditions. Furthermore, the plasma-synthesized catalyst exhibited longer catalytic activity (>20 h) compared to the catalyst synthesized by wet impregnation. The enhanced activity of the plasma-reduced catalyst was attributed to the highly dispersed Pd NPs (nanoparticles) on the support and weaker chemisorption of C_2H_4 on the catalyst surface. As a result, active sites blocked by C_2H_4 were freed, allowing for greater C_2H_2 adsorption, thus improving conversion and C_2H_4 selectivity.

The application of DBD plasma increased the BET-specific surface area of a Ni/CeO_2-Al_2O_3 catalyst from 237 to 254 m^2/g. The catalyst was used for CO_2 hydrogenation to CH_4. The plasma-treated catalyst achieved 85% CO_2 conversion, whereas the untreated sample yielded ~78% CO_2 conversion at 350 °C, as reported by Bian et al. [43]. The improved activity was attributed to an increase in basic sites on the catalyst surface and the uniform dispersion of active Ni^0 particles.

While most studies have focused on the influence of plasma on catalyst properties, it is important to note that the catalyst can also affect plasma discharge. Tu et al. [44] reported that the discharge power increased with the degree of catalyst reduction. The authors reduced Ni/γ-Al_2O_3 in a 20% H_2/Ar mixture with an applied voltage of 24 kV and a frequency of 30–40 kHz. After prolonged treatment (4 h), the maximum H_2 consumption peak was observed at 45 min, after which, it decreased, as seen in Figure 10a. Interestingly, the plasma power also increased from 0 to 110 W up to 45 min and then stabilized, as seen in Figure 10b. This could have been due to more conductive Ni^0 sites forming on the catalyst surface. It was also found that the effective capacitance of the discharge in the presence of non-conductive packing materials (e.g., NiO/Al_2O_3) was lower than that of the discharge packed with conductive materials (e.g., Ni/Al_2O_3). This suggests that the reduction of the NiO to Ni^0 metal phase led to the spatial expansion of the discharge across the gap, potentially caused by an increase in the electric field around the metallic nanoparticles.

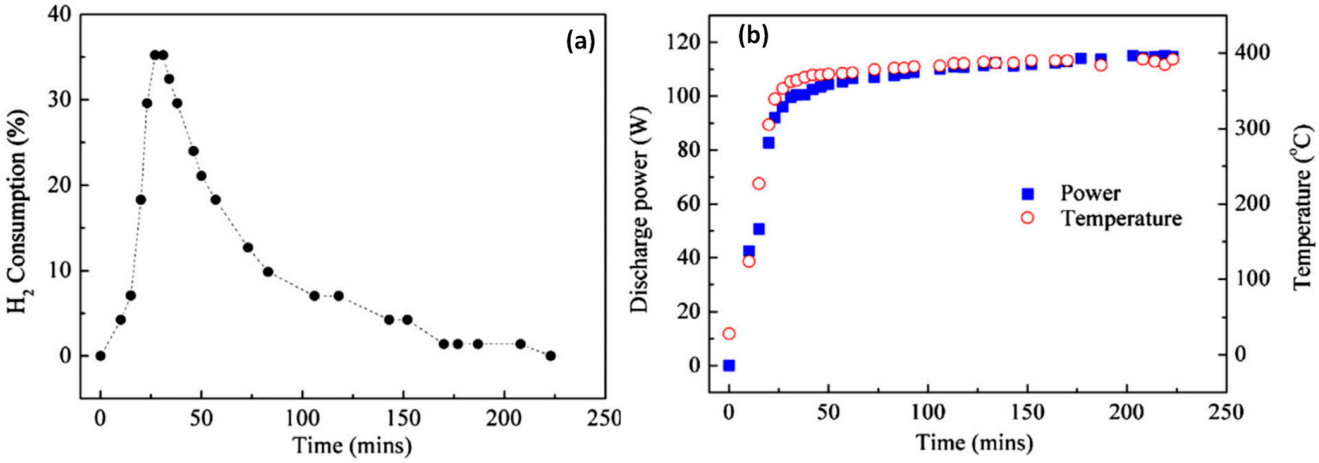

Figure 10. (**a**) H_2 consumption during the reduction of NiO/Al_2O_3 in a 20 vol.% H_2/Ar under DBD discharge. (**b**) Temporal evolution of discharge power and temperature during the reduction of NiO/Al_2O_3 in a 20 vol.% H_2/Ar DBD. Reprinted with permission from [44].

The effectiveness of DBD plasma in tuning the basic sites on a catalyst surface was tested by Benrabbah et al. [45]. The authors loaded 15 wt% of $Ni(NO_3)_2{\cdot}6H_2O$ onto a commercial ceria–zirconia mixed oxide ($Ce_{0.58}Zr_{0.42}O_2$, Rhodia Solvay) catalyst. At a fixed plasma input power of 8 ± 0.5 W and H_2 feed flow of 160 mL/min, a treatment time of 20 min resulted in a total basicity of 212 µmol/g, which increased to 231 µmol/g with 60 min of plasma treatment. The untreated sample exhibited a total basicity of 198 µmol/g. The catalyst was used for CO_2 hydrogenation to CH_4, and the plasma-reduced sample was compared to one that was thermally reduced. Interestingly, the catalytic efficiency for CO_2 conversion reached the maximum as a function of plasma treatment time. The sample treated with plasma for 40 min exhibited a 73% CO_2 conversion, while those treated for 60 and 20 min yielded 61 and 35% CO_2 conversion, respectively. The unexpected trends in catalytic activity were attributed to the varying proportions of basic sites formed on the catalyst surface at different exposure times.

The benefits of DBD plasma in inhibiting the incorporation of Ni^{+2} into the $MgAl_2O_4$ lattice were demonstrated by Fan et al. [46]. The authors synthesized $Ni/MgAl_2O_4$ using DBD plasma with an input power of 200 W for CO_2 hydrogenation to CH_4. The DBD-assisted decomposition resulted in smaller Ni^0 particles with enhanced metal–support interaction. Since DBD assisted in the decomposition of nickel nitrate at a low temperature, it prevented the incorporation of nickel atoms into the $MgAl_2O_4$ lattice. Additionally, a unique structure was formed, which facilitated the hydrogenation of CO_2 to CH_4. In another study on CO_2 hydrogenation to CH_4 using a plasma-modified catalyst, it was observed that plasma treatment significantly enhanced CO_2 desorption capacity and CO_2-to-CH_4 activity at low temperatures compared to the untreated sample. Given that nickel is highly active for hydrogenation, various modifications of the nickel active center on different supports have been explored in the literature. For example, Ni/SiO_2 catalysts synthesized via NH_3 impregnation and plasma decomposition were reported by Zhao et al. [47] for CO methanation. The superior activity of the plasma-treated sample was attributed to the controlled growth of NiO particles at low temperatures through DBD treatment, which led to the formation of a unique Ni catalyst with high dispersion, strong metal–support interaction, and a surface featuring fewer defect sites and more Ni (111) planes.

Plasma-assisted reduction (PAR) was performed on Pt- and Co-based catalysts supported on Al_2O_3, which were subsequently used for CH_4 conversion to hydrocarbons. The plasma–catalytic reaction demonstrated favorable characteristics, producing light alkanes such as C_2H_6, C_3H_8, and C_4H_{10}. In contrast, without plasma treatment, the selectivity towards C_2H_6, C_2H_4, and C_2H_2 was higher. This suggests that PAR effectively reduces supported metal catalysts [48]. In most studies, catalyst treatment was typically performed using either thermal or plasma treatment methods. However, we conducted CO_2 hydrogenation to CH_3OH by coupling plasma with thermal heating, which significantly enhanced reactor performance, resulting in higher CO_2 conversion and CH_3OH production. This improvement was attributed to the plasma-induced spinel phase formation in the catalyst during the reaction, which facilitated CO_2 conversion and CH_3OH production [49–51].

A highly selective $AuPd/TiO_2$ catalyst was prepared using RF plasma treatment, and the hydrogenation of C_2H_2 to C_2H_4 was carried out. At 225 °C, the 30 min plasma-treated sample achieved about 93% C_2H_2 conversion. Moreover, about 75% of C_2H_4 yield was obtained with the plasma-treated sample, compared to only 60% with the thermally calcined sample. These findings emphasize the advantages of plasma treatment in enhancing catalytic activity [52]. The superior performance of the plasma-treated catalyst was attributed to the smaller particle size of active Au metal formed on the surface after plasma exposure.

Similarly, with 130 W input power and 15–45 min of RF plasma treatment, the Pd/TiO_2 catalyst achieved about 85% C_2H_2 to C_2H_4 conversion at 35 °C, whereas the thermally calcined sample exhibited only 75% conversion. The plasma treatment promoted the formation of Ti^{3+} at relatively low temperatures. Furthermore, plasma treatment resulted in stronger interaction between the support TiO_2 and PdO, enhancing the metal–support interaction. This strengthened interaction improved the electronic properties such as electron transport, which enhanced C_2H_2 conversion [53].

The reduction of NiO to Ni due to streamer interaction was observed during the GD treatment of Ni/PVMT by Zhang et al. [54]. The treatment was conducted at 80 V, with a current of 2 mA and a plasma treatment time of 40 min. In addition, plasma treatment resulted in a reduction in NiO particle size and improved uniformity in dispersion. When the catalyst was tested for CO hydrogenation to CH_4, it was observed that plasma treatment significantly reduced the activation energy barrier for CO hydrogenation to CH_4 by 20-fold. At an operating temperature of 450 °C, the plasma-treated sample achieved 93.5% CO conversion with a TOF (turnover frequency) of 0.8537 s^{-1}, while the untreated sample yielded only 16% CO conversion with a TOF of 0.0984 s^{-1}. The authors attributed this enhancement to the dispersion of active Ni atoms over the support. The understanding of catalysis suggests that Ni^0 facilitates the dissociative adsorption of H_2, which then spills over to the CO adsorption sites, promoting CH_4 production. The mass transfer of H_2 is more efficient in catalysts with finer dispersion than in undispersed catalysts.

In a similar study, a Ni/ZrO_2 catalyst was treated with DBD plasma at 200 W of input power and a temperature of 150 °C. The treated catalyst was used for CO hydrogenation to CH_4. The plasma-treated catalyst achieved 100% CO conversion and 100% CH_4 yield at 240 °C, whereas the untreated sample showed only 30% CO conversion and 15% CH_4 yield. This reduction in yield was attributed to carbon deposition on the catalyst surface, which was not converted to CH_4 [55].

Not only inorganic metal oxides, which are resistant to decomposition, but also 15Ni/UiO-66 supported Ni catalysts on metal–organic frameworks (MOFs) were activated with DBD plasma and used for catalytic CO_2 hydrogenation. The authors observed that the plasma-activated catalyst achieved 85% CO_2 conversion and 99% selectivity towards CH_4 compared to the thermally activated sample. This trend was attributed to the lowering of the activation energy barrier for the reaction due to the formation of multiple carbonates and formates on the catalyst surface activated by NTP, which led to superior performance [56]. The effectiveness of plasma in suppressing the formation of $NiAl_2O_4$ was demonstrated by Yu et al. [57]. The authors, upon treating Ni/Al_2O_3 using plasma in oxygen flow, observed that plasma was effective in increasing the dispersion of the Ni catalyst and suppressing the formation of $NiAl_2O_4$. This resulted in a methane space–time yield from CO_2 of 21103.6 $mg{\cdot}gNi^{-1}h^{-1}$ for the plasma-treated catalyst, compared to 6190.5 $mg{\cdot}gNi^{-1}{\cdot}h^{-1}$ for the untreated catalyst at 400 °C.

DBD plasma was also employed for the synthesis of perovskite $La_{0.43}Ca_{0.37}Ti_{0.94}Ni_{0.06}O_{2.955}$ operated at a fixed excitation frequency of 20 kHz and an applied root mean square voltage of 1.2 kV for 10 min. The DBD plasma was supplied with He and He/H_2 mixtures at a flow rate of 6 LPM, with the H_2 concentration in the He/H_2 mixture set at 0, 0.6, and 1%. The authors observed that the H_2 concentration in the feed influenced the nanoparticle's characteristics, specifically by producing smaller and more densely packed nanoparticles. The presence of H_2 affected the metallic phase, which was reduced when hydrogen was absent, indicating that H_2 plays a crucial role in enhancing the exsolution process and the formation of metallic NPs. Hydrogen addition also modified the density and type of surface defects, altering nanoparticle density, chemical composition, and size distribution. Compared to He-only plasma, the filamentary regime observed with H_2 caused spatial inhomogeneities that could accelerate the exsolution process.

The synthesized catalyst was used for (1) CH_4 production from $CO + H_2$, (2) CO oxidation, and (3) CH_4 oxidation. The plasma-treated catalyst exhibited superior performance due to the small size and high dispersion of the Ni NPs, which increased the surface area available for the reaction, leading to higher reaction rates and efficiency. The strong contact between the exsolved NPs and the perovskite support improved the operational stability of the catalyst. The plasma-treated catalysts were well-suited to practical applications due to their stability, which is critical for maintaining catalytic performance over extended periods [58].

Table 5 is a summarized overview of the literature regarding various types of catalysts, the conditions for plasma and thermal modifications, and the performance of modified catalysts for hydrogenation reactions. Table 4 highlights the advantages of plasma treatment over thermal treatment concerning the properties of the catalysts.

Table 5. Comparative table for operating conditions, performance, and advantages of plasma over thermal modification technique for gas phase hydrogenation reaction.

Catalyst	Application	Catalyst Treatment Conditions		Conversion and Yield		Advantage of Plasma-Treated Material over Thermally Treated Materials	References
		Plasma	Thermal	Plasma-Treated	Thermally Treated		
$Fe\text{-}Cu/SiO_2$	CO hydrogenation to alcohol	**GD plasma** (voltage 100 V, frequency 13.56 MHz, and current 50 mA in N_2 atmosphere and then a H_2 atmosphere for 45 min each)	Calcined at 350 °C for 3 h in air	57% CO conversion Selectivity for hydrocarbon 51.7%, CO_2 19%, and ROH 29.3%	36% CO conversion Selectivity for hydrocarbon 57%, CO_2 12.1%, and ROH 30.9%	1.1-fold improvement in surface area, 0.85-fold lowering in average pore size, 1.1-fold lowering in crystallite size leading to synergistic interaction enhancement	[41]
Pd (0.15 wt%)/ $\alpha\text{-}Al_2O_3$	Selective hydrogenation of acetylene to ethylene	**GD plasma** (frequency 13.56 MHz, voltage 100 V, initial pressure of N_2-H_2 plasma 2–200 Pa, and anodic current 100 mA for 85 min)	Calcined at 450 °C for 5 h and then reduced in H_2	Complete C_2H_2 conversion71.3% C_2H_4 selectivity up to 600 °C	No activity under the same conditions up to 600 °C	Higher surface area and improved dispersion lowered the activation energy	[42]
$Ni/CeO_2\text{-}Al_2O_3$	CO_2 hydrogenation to CH_4	**DBD plasma** (plasma operating conditions not specified)	Calcined at 500 °C in air for 4 h	<75% CO_2 conversionCH_4 selectivity 100%	>65% CO_2 conversion CH_4 selectivity 95%	1.1% increased surface area, 1.3% improved metal surface area, 1.2% increased pore volume, ~1.37% enhancement in metal dispersion, ~1.35% lowering in particle size of metal, ~3.5-fold increased basic sites	[43]
33% NiO/Al_2O_3	CO hydrogenation to CH_4	**DBD plasma** (voltage 24 kV, frequency 35 kHz with 20 vol.% H_2/Ar as the plasma working gases and flow rate 100 mL/min for 4 h	-	-	-	Reduction in particle size and better dispersion of metal	[44]
15% Ni/ $Ce_{0.58}Zr_{0.42}O_2$	CO_2 hydrogenation to CH_4	**DBD plasma** (voltage 15 kV 42.5 kHz, power 8 W ± 0.5 W, and H_2 feed flow rate 160 mL/min for 20–60 min	Thermal reduction under H_2 through temperature programmed reduction (5 °C/min) followed by isothermal reduction at 470 °C for 2 h	~73% CO_2 conversionCH_4 selectivity <75%	~61% CO_2 conversion CH_4 selectivity ~55%	Basicity improved by ~1.7-fold, 1.25-fold lowering in Ni crystallite size	[45]
$Ni/MgAl_2O_4$	CO_2 hydrogenation to CH_4	**DBD plasma** (voltage 14 kV, power 200 W)	Calcined at 500 °C for 4 h	<85% CO_2 conversion and selectivity towards CH_4	>85% CO_2 conversion and selectivity towards CH_4	Enhanced surface area and smaller crystallite size of Ni which improved metal–support interaction	[46]
Ni/SiO_2	CO hydrogenation to CH_4	**DBD plasma**, low temperature	Thermal treatment	Superior activity due to high dispersion	75% conversion	High activity and dispersion of Ni atoms	[47]
Pt/Al_2O_3	CH_4 conversion to hydrocarbons	**DBD plasma** (AC pulse power supply (ITM) with 0–10 kV and 10–40 kHz for 2–5 s)	Calcined at 500 °C for 2 h and reduction in H_2 at 400 °C for 4 h	CH_4 conversion 33.3% Higher selectivity towards C_2H_6, C_2H_4, and C_2H_2	CH_4 conversion 25.9%	Complete reduction of Pt, uniform distribution of Pt	[48]
15% $CuO\text{-}Fe_2O_3$	CO_2 conversion to CH_3OH	**DBD plasma** (power 2 W, 100 mL/min 25% CO_2 + 75% H_2, 200 °C	Calcined at 600 °C in air	13.5% CO_2 conversion7.4% CH_3OH yield	>3% CO_2 conversion 1.2% CH_3OH yield	Partial reduction of ferrite, lowering in crystallite size of active metal oxide, plasma-induced formation of oxygen vacancy	[49]
5% $CuO\text{-}Fe_2O_3$		**DBD plasma** (power 2 W, 100 mL/min 25% CO_2 + 75% H_2, 200 °C	Calcined at 600 °C in air	16.7% CO_2 conversion4.64% CH_3OH yield	>3% CO_2 conversion 0.4% CH_3OH yield		[50]
10% $NiO\text{-}Fe_2O_3$		**DBD plasma** (power 7.7 W, 100 mL/min 25% CO_2 + 75% H_2, 200 °C	Calcined at 600 °C in air	9.2% CO_2 conversion5.8% CH_3OH yield	>3% CO_2 conversion 1.1% CH_3OH yield		[51]
$AuPd/TiO_2$	Hydrogenation of acetylene to ethylene	**360° rotating RF plasma** (H_2 plasma with 130 W power for 30 min)	Thermal reduction at 250 °C in H_2 flow for 2 h	<93% C_2H_2 conversion70% C_2H_4 yield	>40% C_2H_2 conversion >40% C_2H_4 yield	Enhanced catalytic activity due to 2-fold improvement in metal dispersion that led to a stronger spillover of H_2 s, a large number of surface Pd sites for acetylene adsorption, and the formation of contiguous Pd ensembles, improving the H_2 chemisorption	[52]
Pd/TiO_2	Hydrogenation of acetylene to ethylene	**RF plasma** (130 W, initial pressure 450 mm, and tor pressure of H_2 gas 15–45 min)	Calcined at 120 °C in air for 12 h	100% C_2H_2 conversion and C_2H_4 selectivity 80%	90% C_2H_2 conversion C_2H_4 selectivity 50%	Distribution of Pd (1 0 0) and Pd (1 1 1) planes changes in Pd/TiO_2, formation of Ti^{+3}, and uniform distribution of metal that led to stronger metal–support interaction	[53]
Ni/PVMT	CO hydrogenation to CH_4	**GD Plasma** (voltage 80 V and anodic current 2 mA for 40 min)	Calcined at 550 °C for 4 h and then thermally reduced with H_2 60 mL/min for 2 h	93.5% CO conversionCH_4 selectivity 64%	64.7% CO conversion CH_4 selectivity 62.4%	Reduced activation energy barrier due to uniform distribution of metal and smaller crystallite size, which led to stronger metal–support interaction	[54]
Ni/ZrO_2	CO hydrogenation to CH_4	**DBD plasma** (power 200 W, voltage 14 kV, and frequency 22 kHz operated at 150 °C in Ar gas flow)	Calcined at 500 °C for 3 h	100% CO conversion100% CH_4 yield	30% CO conversion 15% CH_4 yield	Higher BET surface area, smaller Ni particle size, more homogeneous Ni distribution, stronger Ni-ZrO_2 interaction, more Ni active sites provided favoring H_2 dissociated adsorption, immediate formation of NiO nuclei, which were slowly assembled into clusters and then into particles under a low bulk temperature	[55]
15Ni/UiO-66	CO_2 hydrogenation to CH_4	**DBD plasma** (H_2 as the discharge gas; flow rate 50 mL/min; voltage 5.5, 6.0, and 6.5 kV; frequency 20.3 kHz)	Calcined in a tube furnace at 250 °C under N_2 for 5 h with a ramp of 5 °C/min	85% CO_2 conversion99% selectivity towards CH_4	65% CO_2 conversion 25% selectivity towards CH_4	Lower activation energy barrier by ~32 kJ/mol due to NTP-assisted formation of carbonates and formates on the surface	[56]
Ni/Al_2O_3	CO_2 hydrogenation to methane	Plasma in oxygen flow	Thermal activation	21,103.6 $mg{\cdot}g_{Ni}^{-1}{\cdot}h^{-1}$ methane space–time yield	6190.5 $mg{\cdot}g_{Ni}^{-1}{\cdot}h^{-1}$ methane space–time yield	Greater Ni dispersion (26.5%) and less $NiAl_2O_4$ spinel	[57]
$La_{0.43}Ca_{0.37}Ti_{0.94}Ni_{0.06}O_{2.955}$	Catalytic reactions (CH_4 production, CO oxidation, and CH_4 oxidation)	**DBD plasma** (frequency 20 kHz, voltage 1.2 kV, treatment time 10 min, 8 L/min of He and H_2 mixture feed flow)	Calcined in air at 500 °C for 4 h then thermal reduction with 5% H_2/He at 900 °C for 4 h	Rate of CO conversion 30 mmol/s CH_4 and CO_2 production 140 and 90 mmol/s	Rate of CO conversion 15 mmol/s CH_4 and CO_2 production 70 and 20 mmol/s	Superior performance due to high dispersion, improved operational stability, DBDs resulted in a low-temperature, very fast, and higher growth rate of NPs than conventional hydrogen thermochemical reduction	[58]

4.3. Plasma-Treated Catalyst for the Oxidation of CO and CH_4

Zhang et al. [59] synthesized Ni/α-Al_2O_3 by decomposing a Ni precursor using Ar-RF plasma followed by H_2 plasma reduction. The RF plasma was applied for 90 min at a frequency of 13.6 MHz with 650 Pa of pressure, 160 W of input power, and a fixed flow rate of 20 mL/min. It was observed that the catalyst color changed during the plasma treatment. Initially, the $Ni(NO_3)_2$ was green, which transformed into black-colored Ni_2O_3 and then into green-colored NiO powder. This green NiO was further reduced in a H_2 atmosphere to metallic, black-colored Ni.

The catalytic activity of the plasma-treated sample was compared with the catalyst prepared by calcination (calcined at 900 °C for 10 h and then reduced in a H_2 atmosphere at 600 °C for 1 h). The synthesized catalyst was used for CH_4 conversion to syngas (H_2 + CO) via partial oxidation. Interestingly, at 750 °C, about 93.2% CH_4 conversion was achieved with the plasma-treated sample, while the thermally treated sample yielded 88.6% conversion. This increased activity was attributed to the plasma treatment activating the sample. The thermal treatment led to the formation of a nickel aluminate spinel structure ($NiAl_2O_4$) on the catalyst surface, confirmed by XRD analysis. $NiAl_2O_4$ was inactive towards the chemisorption of H_2 and CO. In contrast to thermal calcination, which consumed more than 1.5 kWh of power, plasma treatment at lower temperatures significantly reduced the total energy consumption of the process [60].

The uniform dispersion of Pt nanoparticles via plasma treatment has been reported to reduce the activation energy barrier for CO oxidation to CO_2, as demonstrated by Nazarpoor et al. [61]. A Pt/γ-Al_2O_3 catalyst was pre-treated with O_2 plasma for 60 min. Plasma treatment enabled 100% CO conversion at 225 °C, whereas the thermally calcined sample achieved 100% CO conversion at 375 °C.

Li et al. [62] synthesized stable, coke-resistant Ni catalysts for the partial oxidation of CH_4 to syngas (CO + H_2). The discharge was initiated using a plate-to-plate AC discharge model under atmospheric pressure at room temperature with an Ar flow. The discharge voltage was set to 40 kV for the plasma treatment. The catalyst not only showed enhanced activity for CH_4 conversion over an extended time (as seen in Figure 11) but also exhibited resistance to carbon deposition. The improved performance of the plasma-treated catalyst was attributed to the homogeneous dispersion of Ni^0 on the catalyst support, which reduced coke formation.

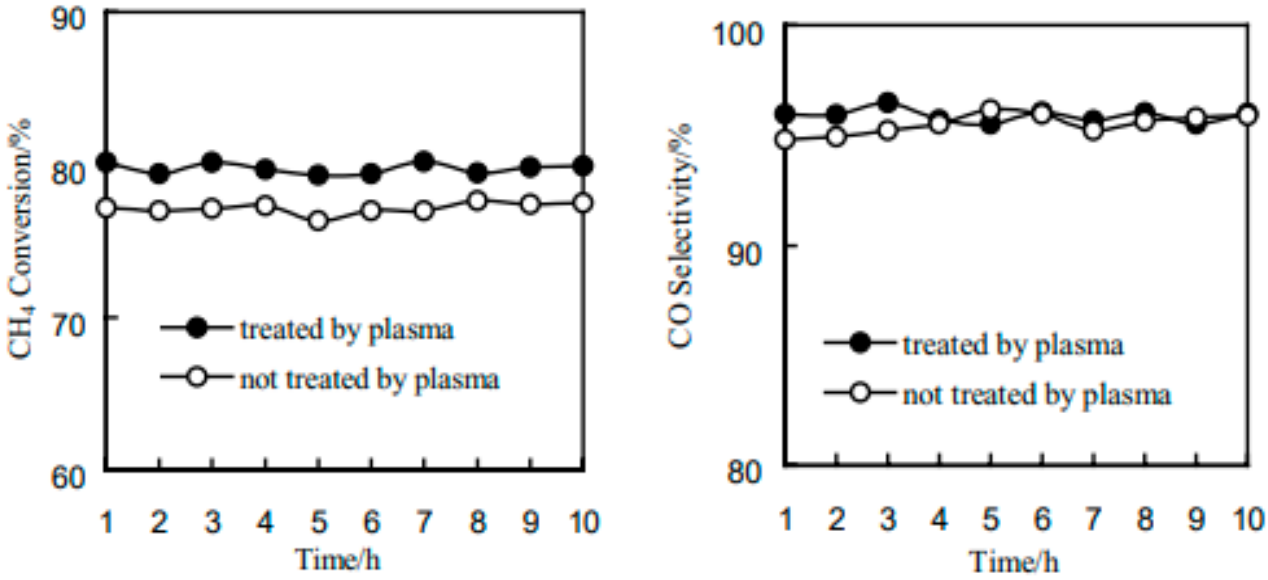

Figure 11. CH_4 conversion and CO selectivity on 5% Ni/γ-Al_2O_3 catalyst. Reprinted with permission from [62].

The activation energy barrier for the partial oxidation of CH_4 to syngas was reduced 16-fold using a plasma-activated catalyst, as demonstrated by Wang et al. [63]. Ar-DC-GD plasma (12 Pa pressure, 1 h treatment) was applied to a Ni-Fe/Al_2O_3 catalyst. The authors suggested that the plasma treatment induced the formation of active Ni species on the catalyst surface, improving its resistance to carbon deposition.

Chen et al. [64] demonstrated that GD plasma treatment in a N_2 atmosphere at a 13.56 MHz frequency led to the enrichment of the Co_3O_4 spinel structure on the surface of a cobalt catalyst prepared by the sol–gel method for CH_4 combustion. The bombardment of highly active plasma species on the catalyst surface disrupted the -Si-O-Co- bonds formed during the sol–gel process, creating a spinel structure and enhancing catalytic performance. Figure 12 presents a comparison between catalysts produced with and without plasma treatment, showing that CH_4 conversion is approximately twice as high in the plasma-treated catalysts.

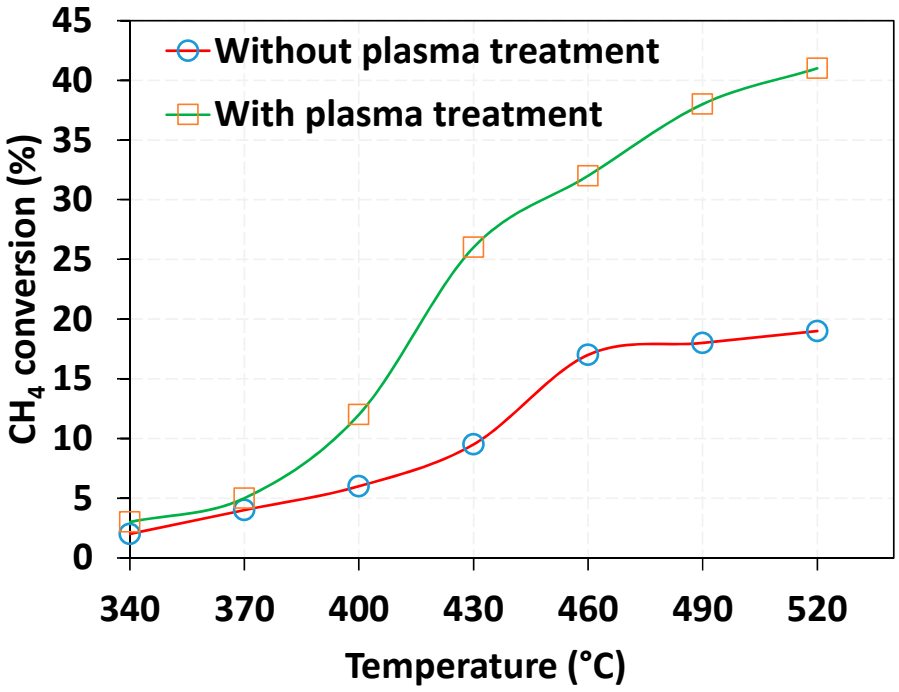

Figure 12. Influence of plasma treatment on catalytic performance [64]. The catalyst was treated in Ar GD for 120 min, with 2 to 200 Pa of pressure, discharge voltage of 100 V, and anodic current of 100 mA at room temperature and then thermal calcination at 470 °C for 4 h.

For the catalytic reaction to occur, the catalyst must first be activated. Traditionally, this activation is achieved through the application of thermal energy. However, plasma treatment can reduce the catalyst activation temperature, as observed by Qi et al. [65]. The authors activated a Pd/C catalyst using a 50% H_2/Ar mixture operated at 36 kV of AC high voltage and a 14.1 kHz frequency for 6 min. The plasma-treated samples exhibited particles with an average diameter of less than 5 nm, while the thermally treated samples showed an average diameter of 5–15 nm, as seen in Figure 13c,d. The synthesized catalyst was used for CO oxidation to CO_2.

As seen in Figure 14, the plasma-treated samples achieved 100% CO conversion at 100 °C, whereas the thermally treated samples required a temperature of 150 °C to reach the same conversion. The XRD patterns of activated carbon, Pd/C-PC (calcined at 300 °C in H_2 for 2 h), and Pd/C-PW (washed with deionized water and dried at 120 °C for 3 h) are displayed in Figure 13b. All samples exhibited broad carbon peaks at 25.0° and 43.5°. On the surface of the Pd/C-PC, smaller Pd nanoparticles were evenly distributed on the activated carbon.

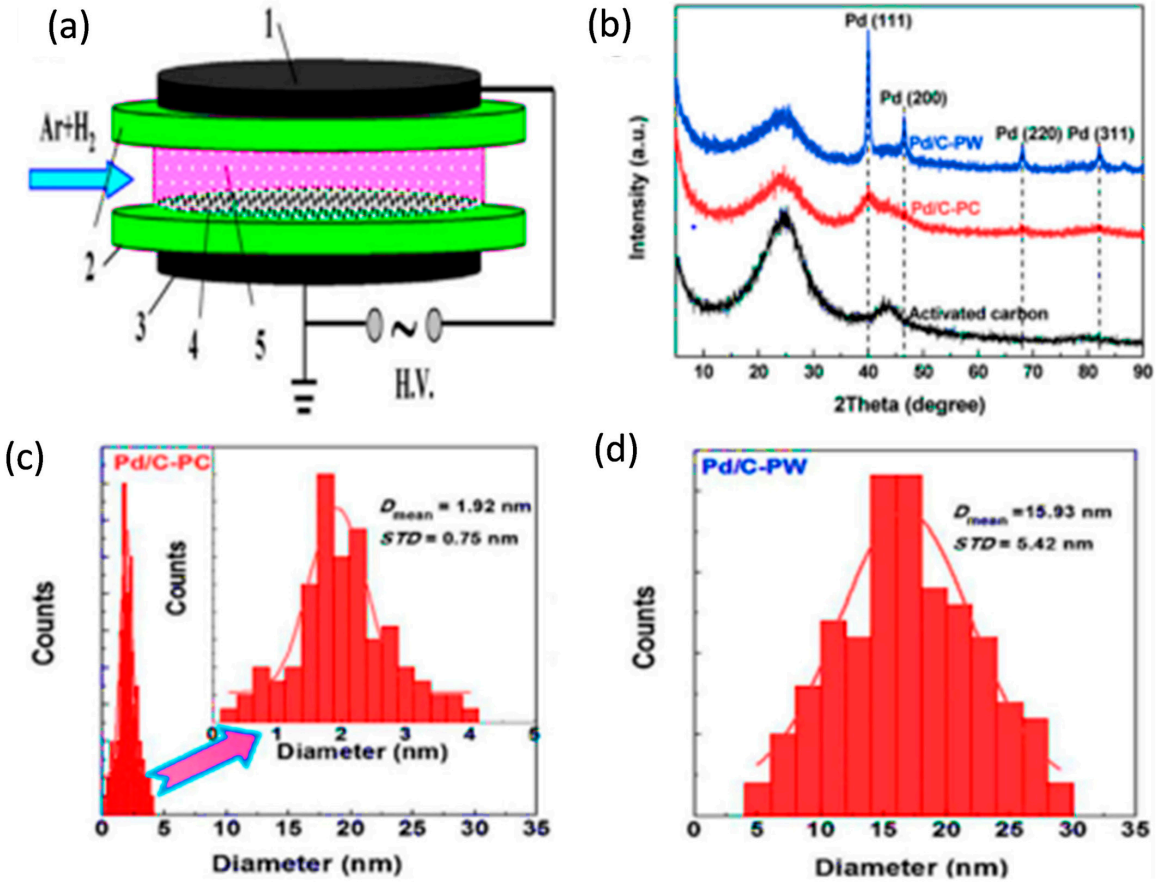

Figure 13. (**a**) Schematic of the DBD cold plasma reactor (1—high voltage electrode, 2—quartz glass, 3—low voltage electrode, 4—sample, and 5—cold plasma). (**b**) XRD patterns of Pd/C-PW, Pd/C-PC, and activated carbon. (**c**) Particle size distributions of Pd-NPs on Pd/C-PC. (**d**) Particle size distributions of Pd-NPs on Pd/C-PW [65].

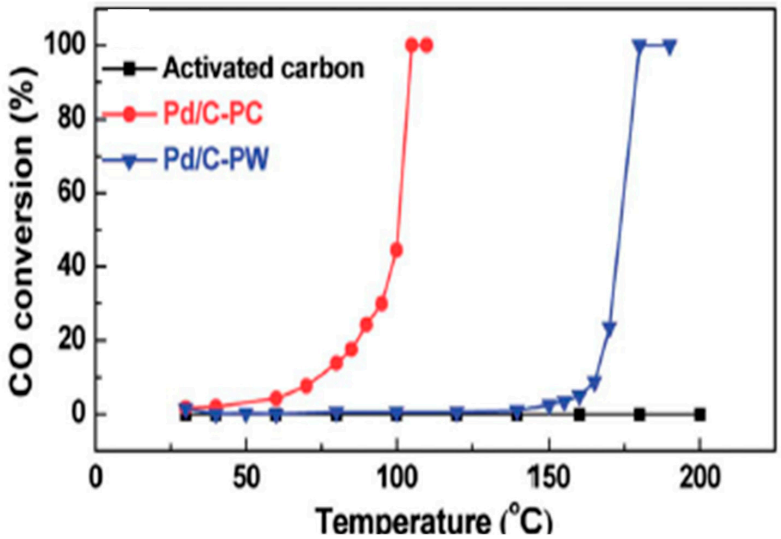

Figure 14. CO conversion over activated carbon, plasma-treated (Pd/C-PC) and thermally treated (Pd/C-PW). Reproduced with permission from [65].

In most studies, H_2 and/or Ar are commonly used as treatment gases for reduction. However, C_2H_5OH has also been used as a reducing gas (H_2 source) to reduce Pd/TiO_2 P-25, as demonstrated by Di et al. [66]. The authors bubbled Ar gas through C_2H_5OH,

and the gas was passed through a DBD reactor packed with a 0.3 g Pd/P-25TiO_2 catalyst. The plasma was ignited with a 9.5 kV applied voltage and 15 kHz frequency; the average power was 14.4 W. The XPS characterization of the catalyst showed that Pd existed in its metallic form after plasma treatment. Additionally, after the plasma treatment, the catalyst was calcined, and the average particle diameter was 1.6 nm, which was smaller than the thermally H_2-reduced catalyst (2.5 nm). This demonstrates that plasma-induced changes are persistent, and catalysts remain stable even after calcination.

CO oxidation was carried out using the synthesized catalyst, and the plasma treatment reduced the catalyst activation temperature. In another study, O_2 was used as a reducing gas by Di et al. [67]. The CO oxidation catalyst Au/TiO_2 was treated with DBD plasma in an O_2 atmosphere. Plasma treatment resulted in the complete reduction of Au, leading to enhanced catalytic activity compared to untreated samples. The study demonstrated that the reducibility of metallic precursors depends on the standard reduction potential of the M^{n+}/M° pairs rather than the carrier gas. It has been suggested that the reduction can only occur when the standard potential is positive. For example, $PdCl_2$ (Pd^{+2}/Pd°, E° = +0.92 V) can be reduced by plasma treatment, whereas $Ni(NO_3)_2$ is oxidized and cannot be reduced to Ni° directly because the standard potential of Ni^{+2}/Ni° is −0.25 V [68].

In another study, O_2-GD plasma was used to understand whether the gas or plasma species contributed to the reduction of active metal catalysts, specifically for a Pd/HZSM-5 catalyst. CH_4 oxidation was studied using the plasma-treated catalyst, which exhibited 100% CH_4 conversion (1.5 Vol% feed concentration) at 425 °C for 10 h. Although O_2 was a carrier gas, the plasma treatment reduced the Pd precursor to metallic Pd^0 (4 nm particle size) rather than causing surface oxidation. This result emphasizes that, with GD plasma, the catalyst was reduced by the electrons available in the discharge zone rather than by the feed gas [69].

The usage of different catalysts, their modification conditions via plasma and thermal treatment, and their effects on the oxidation of GHG are highlighted in Table 6.

Table 6. Comparative table of operating conditions, performance, and advantages of plasma over thermal modification techniques for gas-phase oxidation.

Catalyst	Application	Catalyst Treatment Conditions		Conversion and Yield		Advantage of Plasma-Treated Material over Thermally Treated Materials	References
		Plasma	Thermal	Plasma-Treated	Thermally Treated		
Ni/∝-Al_2O_3	CH_4 conversion to syngas	**Ar-RF plasma** (90 min, 13.6 MHz, 650 Pa, 160 W, 20 mL/min)	Calcined at 900 °C for 10 h, reduced in H_2 at 600 °C for 1 h	CH_4 conversion 93.2%	CH_4 conversion 88.6%	Lower energy consumption, improved activity	[59]
Pt/∝-Al_2O_3	CO oxidation to CO_2	**O_2 RF plasma** (residual pressure 0.3 Torr, power 250 W, and total O_2 flow of 25 mL/min for 60 min then in H_2 at 300 °C for 1 h)	Calcined at 500 °C for 4 h followed by thermal reduction in H_2 at 300 °C for 1 h	CO conversion of 100% at 225 °C	No catalytic activity (thermal)	The smaller particle size of the Pt (2 nm) and Pt-Pt bond remained intact, complete organics removal, formation of partially oxidized Pt species, 50% reduction in sintering, which increased the active sites on the catalyst surface	[61]
Ni/γ-Al_2O_3	Partial oxidation of CH_4	**CD plasma** (plate-to-plate AC discharge, 40 kV, atmospheric pressure, Ar flow 20 mL/min)	Calcined at 400 °C for 4 h, then calcined at 800 °C for 8 h; finally, the sample was reduced at 500 or 800 °C by H_2 for 2 h	CH_4 conversion <70%	CH_4 conversion >70%	Enhanced activity and resistance to coke formation by increased Ni^0 species on the catalyst surface	[62]
Ni-Fe/Al_2O_3	Partial oxidation of CH_4	**Ar-DC-GD plasma** (12 Pa and 1 h, then calcinations at 600 °C for 6 h	Calcined at 600 °C for 6 h	CH_4 conversion <70% at 700 °C	CH_4 conversion >70% at 700 °C	Improved activity and carbon deposition resistance due to Ni^0 dispersion on the catalyst surface, breakage of formed –Si–O–Co– bonds, and the formation of Co_3O_4	[63]
CO_3O_4	CH_4 combustion	**N_2-GD plasma** (frequency 13.56 MHz, discharge voltage 100 V, anodic current 100 mA, total time of plasma treatment 120 min, and a vacuum between 2 and 200 Pa and then calcined at 470 °C for 4 h	Calcined at 470 °C for 4 h	CH_4 conversion 40%	CH_4 conversion >20%	Removal of water and carbonaceous species from silica gel and the partial decomposition of cobalt nitrate took place at lower temperatures	[64]
Pd/C	CO oxidation	**DBD plasma** (mixture of Ar (>99.999%) and H_2 (>99.999%) with a total flow rate of 100 mL/min was used as the working gas in a 50% H_2/Ar mixture, with 36 kV AC and 14.1 kHz for 6 min, followed by washing with deionized water and drying at 120 °C for 3 h)	Calcined at 300 °C in H_2 for 2 h	100% CO conversion at 100 °C	No CO conversion at 100 °C	Reduced activation temperature due to smaller particle size and distribution of Pd nanoparticles, the oxygen-containing functional groups on the surface of the activated carbon due to plasma treatment facilitated the distribution of the Pd nanoparticles	[65]
Au/TiO_2	CO oxidation	**DBD plasma** (voltage 36 kV, frequency 14.5 kHz, power 65.5 W, mixture of Ar (>99.99%) and H_2 (>99.99%) as the working gas, total flow rate of 100 mL/min, treatment time 2 min)	Calcined at 300 °C	100% CO conversion at 15 °C	90% CO conversion at 15 °C	Complete reduction of Au leading to enhanced activity	[66]

4.4. Other Miscellaneous Applications of Material Treatment with Plasma

Plasma treatment has been shown to favor the migration of Ni^{+2} species from the bulk to the surface of the catalyst in a Ni-Ir/γ-Al_2O_3 catalyst. Although the authors did not explain the Ni^{+2} migration mechanism, it can be speculated that the potential difference between the catalyst surface and bulk could be a driving force for the migration of charged Ni species, leading to enhanced NH_3 removal. The catalyst treatment was performed at 175 V with a N_2 + H_2 reducing mixture for 10 min. The plasma-synthesized catalyst exhibited about 90% NH_3 conversion, while the thermally treated sample showed only 80% NH_3 conversion at 600 °C and 1 atm of pressure [70].

Plasma-treated samples also demonstrated superior performance in nitrate (NO_3^-) and nitrite (NO_2^-) reduction in water and gas-phase reactant conversion. A Pt-loaded polypropyl (PPy) polymeric material was treated with Ar-RF plasma, and the efficiency of the plasma-reduced sample was compared to a catalyst reduced by $NaBH_4$. Ar plasma effectively reduced Pt-ions in the chloroplatinum complex to metallic Pt^0 due to the direct transfer of abundant electrons in the plasma to Pt anchored on the PPy surface compared to $NaBH_4$ reduction. Increasing the plasma input power from 100 to 200 W increased the number of carboxylate groups and led to a more effective reduction of platinum ions to zero-valent metallic Pt. Notably, the Pt/PPy obtained after Ar plasma treatment at 200 W showed a 50% reduction in NO_3^-, with acceptable limits of NH_4^+ and NO_2^- formation [71].

The natural goethite iron oxide mineral α-FeO(OH) was treated with GD plasma by using a 1150–1200 V DC voltage at 53 Pa of pressure. The treated catalyst was tested for sulfasalazine antibiotic degradation, and, compared to the untreated catalyst, the Ar plasma-treated catalyst led to enhanced conversion and degradation. These improvements were attributed to an increase in the specific surface area of goethite and the density of surface hydroxyl groups. The increased hydroxyl groups led to the generation of enhanced radicle species, which contributed to the improvement in conversion [72].

Roy et al. [73] prepared a Ni/Al_2O_3 catalyst using 30 min of N_2 RF plasma and tested it for aqueous-phase C_2H_6O reforming. The plasma-treated sample showed about 5.7% more C_2H_6O conversion and higher syngas production than the untreated sample. The authors attributed the enhanced activity to two key modifications: (1) RF plasma treatment removed H_2O molecules and OH groups, exposing more defect centers on the surface, which increased the density of the active acidic centers, and (2) the collision of excited N_2* with Al_2O_3 could form NH_3 on the surface, increasing the basicity of the powder by attracting electrons from Al atoms [74].

Liu and Bai [75] employed Ar-GD plasma, operated at 100 Pa, to reduce a Pd/C catalyst for the Suzuki–Heck reaction. The study found that plasma reduced the Pd nanoparticles, which were well dispersed with a smaller particle size than in untreated samples. Remarkably, the synthesized catalyst showed no loss in catalytic activity even after eight cycles, indicating excellent reproducibility and durability of the plasma-treated catalyst. In another study, Li et al. [76] synthesized Ag nanoparticles (Ag NPs) on a cotton surface using 3 min of Ar-GD at 600 V, 100 Hz, and 12 W of applied power. As shown in the TEM images in Figure 15, the average particle size was 5.3 nm, with an average lattice spacing of 0.235 nm, indicating high crystallinity of the Ag NPs. The average diameter of the Ag NPs increased slightly with the increasing concentration of $AgNO_3$ solution, demonstrating the potential of electron reduction for controlling nanoparticle size. Furthermore, the synthesized nanoparticles exhibited significantly better antibacterial activity, attributed to the smaller Ag particle size. This suggests that low-pressure GD can effectively synthesize size-controlled noble metal nanoparticles supported on material for environmental applications.

Wang et al. [77] synthesized highly dispersed metal (Pd, Pt) nanoparticles and produced uniform Au and Ag nanowires in ordered mesoporous silica SBA-15 using a novel GD plasma treatment. The calcined SBA-15 was impregnated with an aqueous solution of the metal precursor, and the resulting sample was then reduced by GD plasma (treatment time 45 min, pressure 100–200 Pa, 900 V, and 100 Hz frequency). The incorporation of metals

led to a decrease in the specific surface area. The GD plasma was operated at 100–200 Pa with 1 kV of applied potential and a frequency of 100 Hz. During plasma treatment, the authors observed distinct color changes, which directly showed metal nanostructure formation in the SBA-15. The authors suggested that the energy required for plasma reduction is around 38% lower than that needed for thermal reduction.

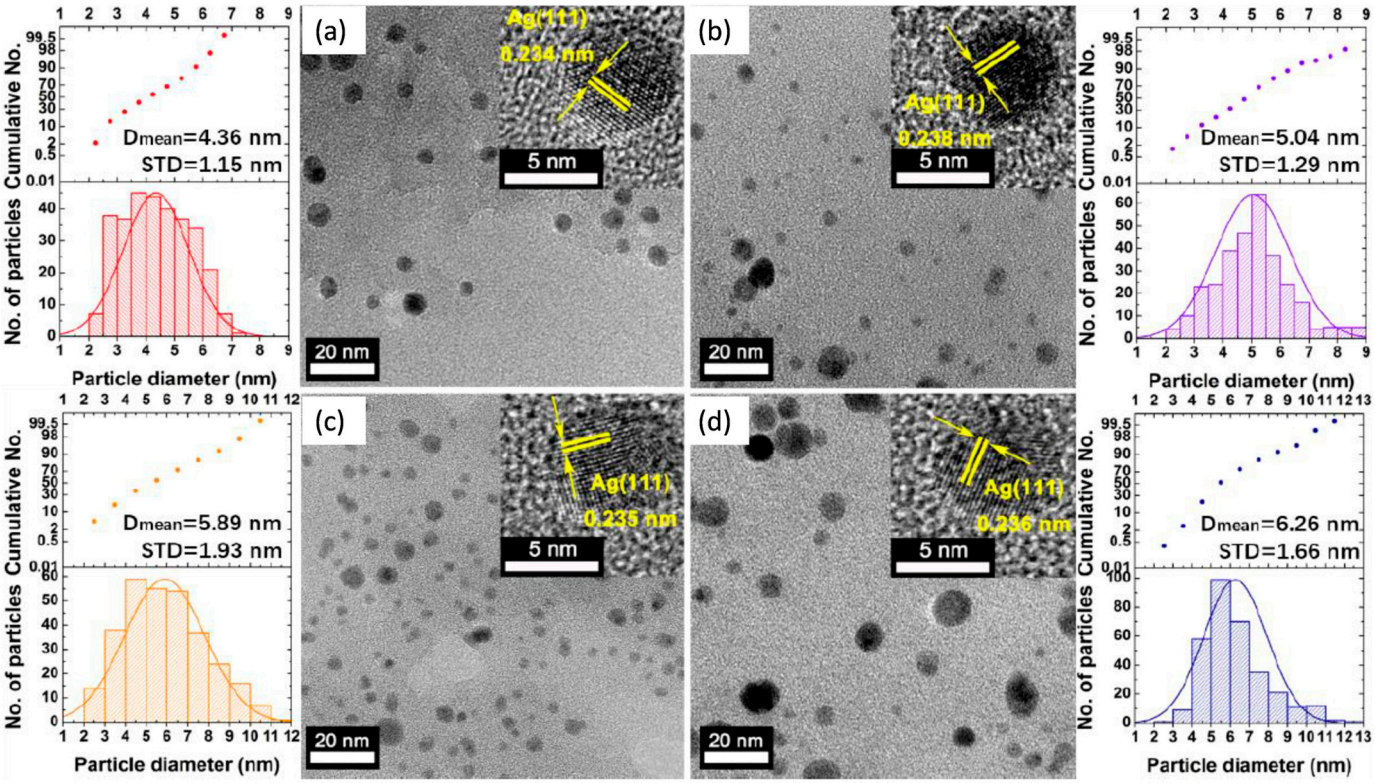

Figure 15. TEM images and histograms of silver nanoparticles on (**a**) Ag/Cotton-1, (**b**) Ag/Cotton-2, (**c**) Ag/Cotton-5, and (**d**) Ag/Cotton-10. The insets of panels (**a**–**d**) display the corresponding high-resolution TEM images of Ag nanoparticles. Reproduced with permission from [76].

Furthermore, the authors proposed that the reduction process was facilitated by two mechanisms:

(1) Plasma-generated electrons reduced the metal ions to metal through the recombination route.

(2) The authors speculated that SBA-15 might contain some moisture, and the water molecules could dissociate into hydrated electrons e_{aq-} and $H^{\bullet}$ radicals. These species are very strong reducing agents and could reduce the metal ions into metallic nanoparticles or nanowires.

In another study, applying GD plasma was shown to reduce catalyst treatment time by 1.5-fold, which could lower gas consumption and make plasma treatment a more environmentally friendly approach due to reduced power consumption. In the conventional method, the catalyst must be treated at 750 °C for 2 h, whereas GD plasma achieved the same result in just 10 min at 25 °C [78]. These results highlight the advantages of GD plasma, offering the desired outcomes with significantly shorter treatment times. The reduced treatment time improves energy efficiency and lowers the reliance on fossil fuels. Plasma application is also aligned with the principles of green chemistry, as it avoids harsh operating conditions. Additionally, plasma illumination creates localized charges on the catalyst surface and generates an electrical field within the solid and at the gas–solid interface. The reactants interact with these charges through electron and/or energy transfer processes, often producing charged molecules that further react with these surface charges.

A Helmholtz layer forms at the interface, and an electrical field is created within the solid due to the presence of surface charges [79].

The schematic in Figure 16 illustrates the spatial profile of long-distance plasma catalysis and nanoscale plasma catalysis. The interaction of species in plasma catalysis and during catalyst modification may resemble those in catalytic application. In porous catalysts/materials, the electric field will be more assertive near void edges and inside the voids during treatment. This enhancement can also alter discharge characteristics, differing from those in the bulk region. Local inhomogeneity and charge distribution are further promoted by applying an electrical potential. The high intensity of the electric field can lead to the generation of different species and active sites, such as electronic defects, which are not observed in the bulk.

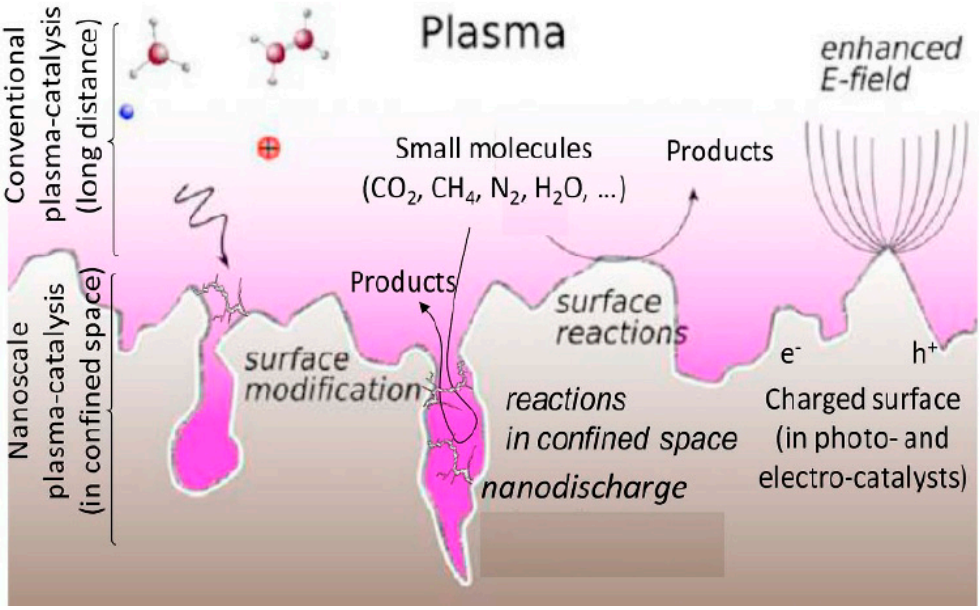

Figure 16. Schematic for conventional plasma catalysis (long–distance interaction), nanoscale plasma catalysis (in confined nano space, range of about 1 to 20 nm), and plasma catalysis interaction with the charged catalyst surface. Reproduced with permission from [79] (The ball stick model is used tio depict atoms wherein the central atom namely carbon is depicted by red ball, small speahers in gray colour infers hydrogen atoms).

Zou et al. [80] demonstrated that plasma treatment can be crucial in preventing the diffusion of active metal from the surface into the bulk of the support. A catalyst was treated with GD plasma to improve metal–support interface interaction, which is crucial for an efficient photocatalytic processes. NiO/Ta_2O_5 and NiO/ZrO_2 catalysts were prepared via Ar-GD, followed by reduction at 500 °C and subsequent oxidation at 200 °C. These catalysts were tested for photocatalytic water splitting. The plasma-treated samples produced approximately twice the yield of O_2 and H_2 compared to the calcined catalyst under similar operating conditions. Remarkably, extensive catalyst characterization revealed that GD discharge at room temperature prevents the diffusion of Ni atoms into the support. As can be seen in Figure 17a,b, the catalysts calcined at 327 °C for 1 h exhibited diffused interfacial regions. This confirmed that thermal treatment led to the thermal diffusion of Ni atoms into the support. However, in the GD plasma-treated catalysts shown in Figure 17c,d, no diffusion of Ni atoms was observed. These findings highlight that plasma treatment can effectively prevent the thermal diffusion of Ni atoms.

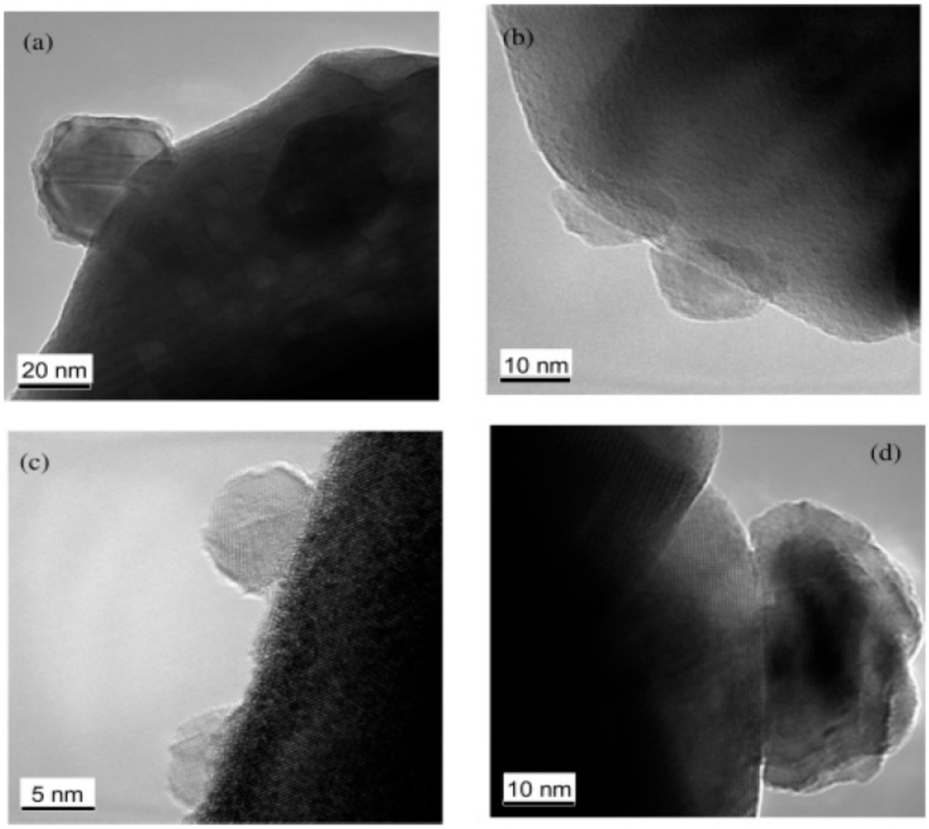

Figure 17. Effect of Ar-GD on improving the metal–support interface. TEM images of calcined (**a**) $Ni(NO_3)_2/Ta_2O_5$ and (**b**) $Ni(NO_3)_2/ZrO_2$ and plasma-treated and calcined (**c**) $Ni(NO_3)_2/Ta_2O_5$ and (**d**) $Ni(NO_3)_2/ZrO_2$. Reprinted with permission from [80].

The aerobic oxidation of benzyl alcohol was carried out using a Au-Pd/SBA-15 catalyst treated with GD plasma. The plasma was operated at 100 Pa with a 1 kV applied voltage. The Ar-GD plasma-treated sample exhibited superior performance compared to the untreated sample due to the presence of more surface-coordination-unsaturated Pd atoms in the catalyst, which significantly boosted its activity compared to H_2 thermal reduction at elevated temperatures. In addition, plasma processing at ambient conditions resulted in uniform particles, improved atom efficiency, and controlled particle morphology [81].

Yu et al. [82] used the CD-enhanced chemical vapor deposition (CVD) technique to synthesize NiO-embedded carbon nanotubes (CNTs) at atmospheric pressure. A mixture of CH_4 (2 mL/min) and H_2 (20 mL/min) was used as the reactants for CNT synthesis. The study showed that the CD technique shortened reduction time and led to smaller NiO particle size formation compared to conventional methods. Moreover, CD enhanced the formation of metallic Ni on the CNT walls.

Interestingly, Li et al. [83] used the CD plasma-enhanced CVD technique to prepare carbon nanotubes on an anodic aluminum oxide (AAO) template. The CD was generated using a tungsten needle and a circular plate. The needle electrode was positioned about 5 mm above the AAO template. The reactants, CH_4 and H_2, in a 1:10 ratio, were fed into the reactor at a total feed rate of 22 mL/min. Plasma discharge was generated using an AC high-voltage generator operating at 4 kV and 25 kHz, with a cumulative plasma input power of 20 W. The study reported that the modifications to the CD reactor significantly increased the nanotube array area and enhanced CNT length.

In another study, Nobuzawa et al. [84] reported the formation of a CNT forest at the tip of one of the electrodes. The schematic of the rector setup is reported in Figure 18a. The CD was generated by applying a potential between a needle cathode and a rod anode (made of graphite), with both electrodes coated with a 60 nm thick layer of Ni. The CD

was generated at atmospheric pressure under H_2 gas mixed with 1% C_2H_4 at 600–800 °C. The mean diameter and length of the obtained multiwall carbon nanotube (MW-CNT) were 30–80 nm and 1–10 µm, as shown in Figure 18b,c. The study also demonstrated that without CD, CNT growth occurred at a higher temperature range (800 to 1000 °C), resulting in fewer straight CNTs.

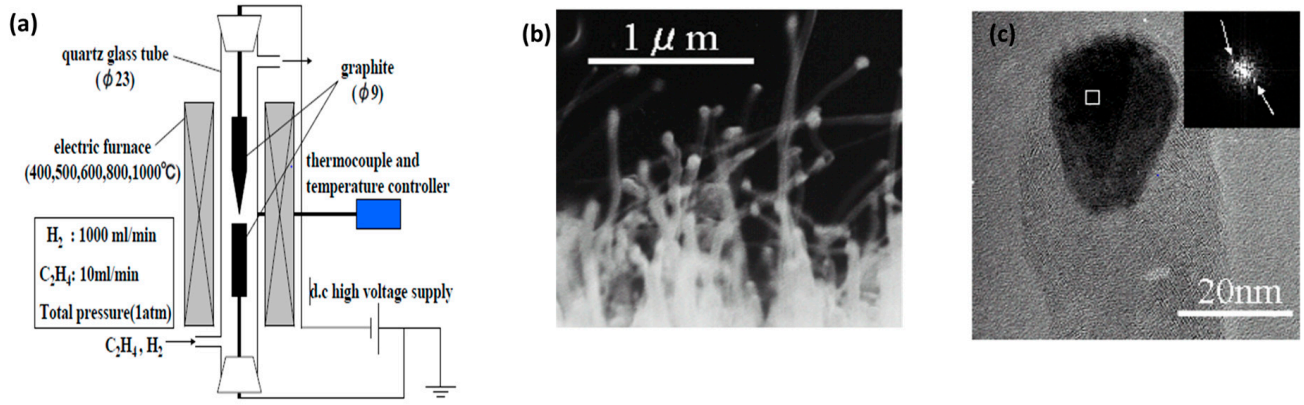

Figure 18. (**a**) Experimental schematic to fabricate CNT forest. (**b**) FESEM image of CNTs formed on graphite needle cathode. (**c**) TEM image of CNTs formed on graphite needle cathode by CD. Experimental conditions: H_2 mixed with C_2H_4 (1%), the temperature at the CD plasma was 800 °C. Reprinted with permission from [84].

Bhattacharyya et al. [85] used a nanoscale CD to achieve localized nanoparticle deposition at the tip of an electrode. A variety of metal nanoparticles (NPs) can be synthesized even with a single short pulse lasting 20 ns or less. The non-thermal CD in liquids leads to the localized deposition of NPs on the electrode tip surface or near the tip on a substrate placed in the liquid. By connecting an ultra-sharp electrode tip to the negative pole of the power supply, a nanosecond duration NTP was generated at the electrode tip by applying voltage pulses. With just a single pulse, the CD reduced Au^{+3} to Au^0 (E^0 = 0.9 V) in the $HAuCl_4$ solution near the electrode tip, leading to the nucleation and growth of NPs within a short duration of the ns pulse, as shown in Figure 19. In a very similar work, diamond nanoparticles were synthesized using CD in an aqueous solution. The authors used a needle-to-plate configuration, igniting discharge at 27 kV and a 50 Hz frequency [86].

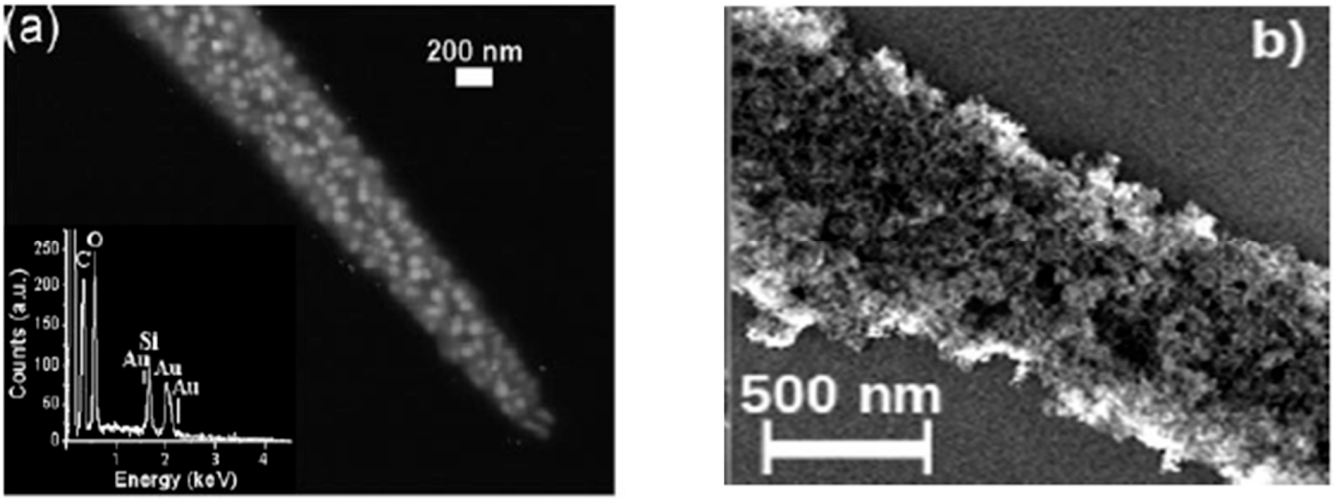

Figure 19. (**a**) Deposition of Au nanoparticles on the ultrafine needle-like electrode from an aqueous solution of a metal precursor [82]. (**b**) Deposition of NPs on needle electrode from a metal precursor solution. Reprinted with permission from [80].

Khataee et al. [87] reported the application of CD for the preparation of Zeolite nanorods. The synthesized catalyst was used for the degradation of phenazopyridine in a heterogeneous sono–Fenton-like process. The treatment was carried out in a reactor consisting of two stainless steel electrodes, with a 30 kV voltage and 300 Hz frequency. The clinoptilolite particles were washed with distilled water and dried at 60 °C for one day. Then, the dry clinoptilolite powder (3 g) was placed in the reactor and modified by the CD for 10 min. Notably, the plasma treatment resulted in a rod-like structure in the nanometer range, as shown in Figure 20.

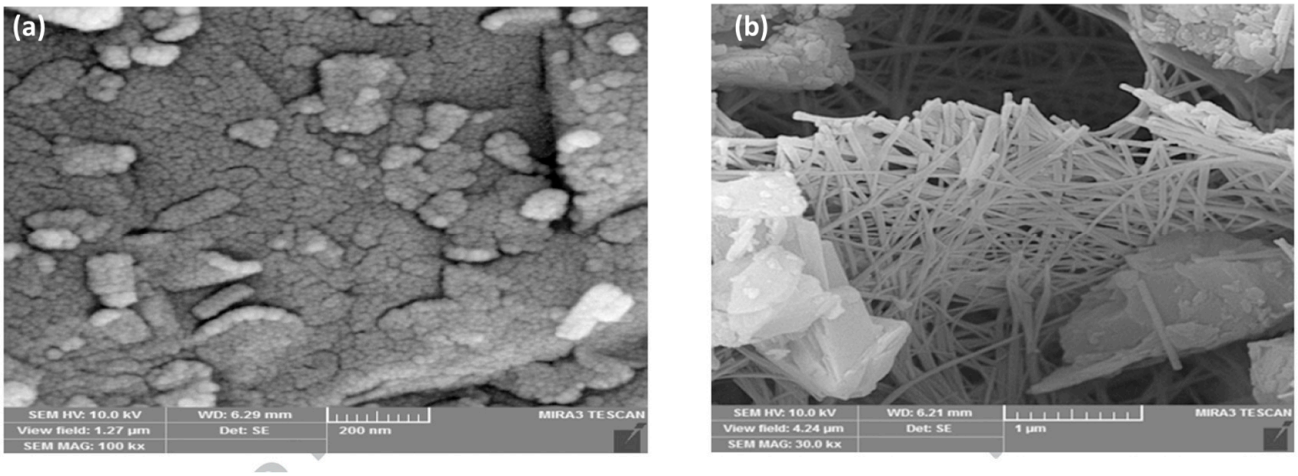

Figure 20. (**a**) Clinoptilolite before treatment. (**b**) Clinoptilolite nanorods after plasma treatment. Reprinted with permission from [82].

Solution plasma is a type of atmospheric nonequilibrium plasma created through electrical discharge in liquids at room temperature. Its adjustable configurations, electrode materials, and power supply characteristics allow for precise control over the size, shape, and composition of the resulting products. This makes solution plasma a valuable tool for synthesizing and modifying advanced materials, particularly in energy conversion applications [88]. Kim et al. [89,90] demonstrated that solution plasma offers a greener route for the synthesis of MnO_2 NPs, as shown in Figure 21. The authors used reducing sugars (glucose, fructose, and sucrose) as both reducing agents and promoters for the formation of MnO_2. The $KMnO_4$ served as the precursor for MnO_2 synthesis, and plasma was ignited using a bipolar pulse power supply with a frequency of 20 kHz and a pulse width of 2 µS for a treatment duration of 10 min. The resulting material was used for the removal of cationic dye from wastewater. In another work, the authors investigated the influence of plasma treatment time on MnO_2 formation using the setup described by Petrović et al. [91] as shown in Figure 22. They observed that 18 min of plasma treatment resulted in the highest absorption intensity for MnO_2 [92].

Even though CD plasma shows promise for material synthesis, this technique has several limitations. For example, CD can only be applied to non-conductive substrates. Additionally, non-uniformity in treatment caused by heterogeneity and suboptimal interaction between the discharge volume and the surface makes the application of CD in catalyst synthesis less straightforward.

The effects of plasma, such as reducing the band gap, increasing the surface area, creating oxygen vacancies, and increasing the concentration of Ce^{+3}, were observed by Petrović et al. [91]. These changes had a positive impact on the degradation of reactive blue 19 dye compared to the untreated catalyst. Boruah et al. [93] used CD plasma to generate oxygen vacancies in a WO_{3-x} catalyst at electron-rich oxygen vacancy sites on the crystal planes and grain boundary defects. The defect-induced vacancies reduced the bandgap from 2.54 to 2.15 eV.

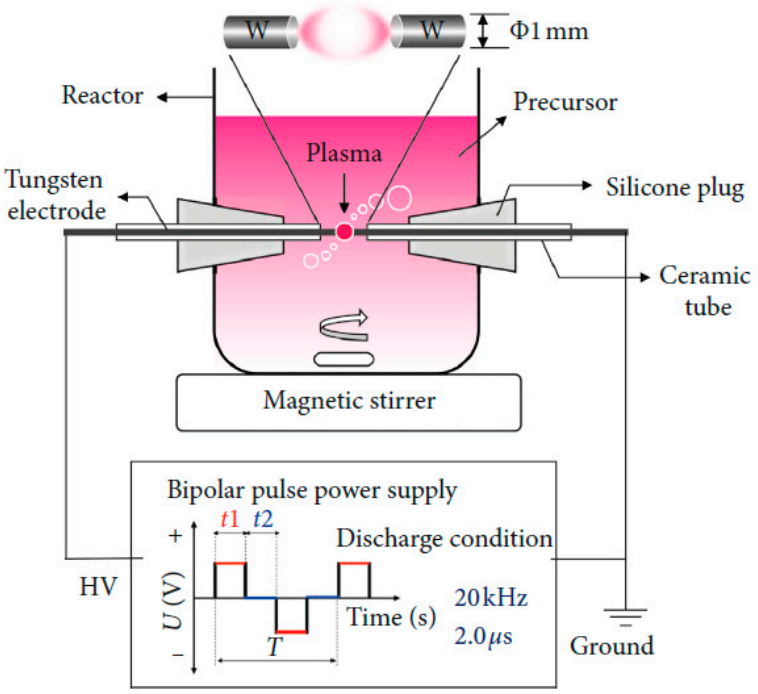

Figure 21. Schematic of the solution plasma (SP) experimental setup. Reprinted with permission from [91].

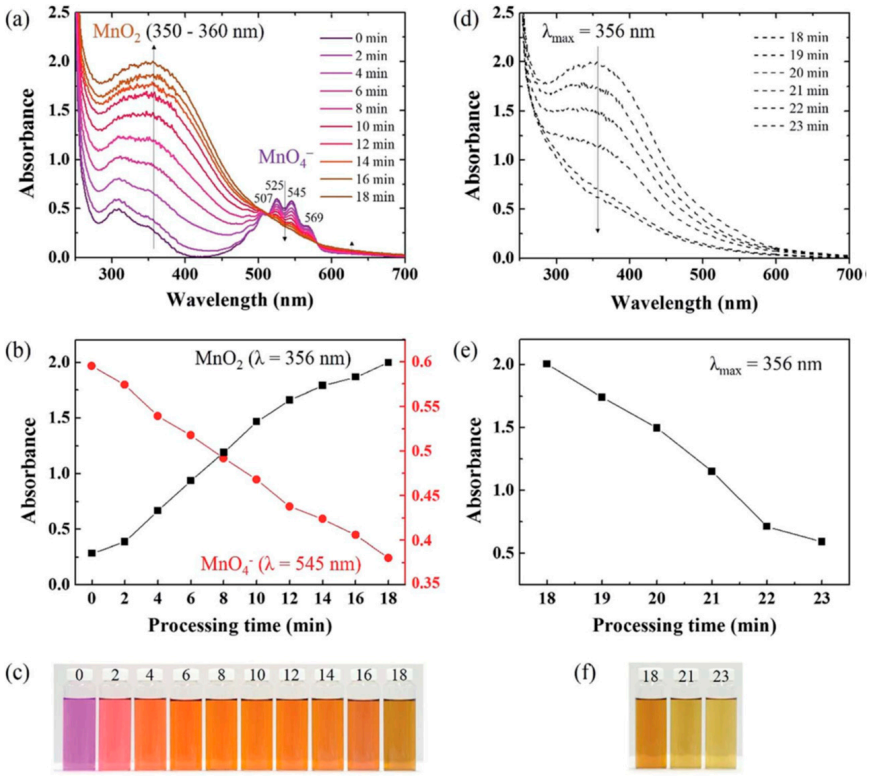

Figure 22. (**a**) UV–vis absorption spectra of the SP-treated $KMnO_4$ aqueous solutions with discharge times of 0–18 min, along with (**b**) time–absorbance plots of MnO_2 (■ 356 nm) and $MnO_4{}^{-2}$(● 545 nm) and (**c**) photographs of the obtained solutions as a function of discharge time. (**d**) UV–vis absorption spectra of the solution during the discharge times of 18–23 min, along with (**e**) time–absorbance plots (■ 356 nm) and (**f**) photographs of the obtained solutions. Reprinted with permission from [92].

Zhao et al. [94] synthesized CdS/Al_2O_3 and ZnS/Al_2O_3 using DBD plasma with a feed flow of 80 mL/min of 10% H_2S/Ar ($Cd(NO_3)_2$ and $Zn(NO_3)_2$ were used as precursors for the wet impregnation process, respectively). The plasma was initiated using a 10 kV voltage, 10 kHz of frequency, 25 W of input power, and a plasma irradiation time of 10 min. The plasma-synthesized catalyst exhibited larger surface areas compared to the thermally calcined samples, as plasma treatment prevented the agglomeration of active components on the catalyst. Moreover, the particle size of Cd in the plasma-treated sample was smaller than in the thermally treated samples. The catalysts were used for H_2S decomposition to produce H_2 gas. Interestingly, both CdS/Al_2O_3 and ZnS/Al_2O_3 achieved 100% H_2S conversion, with dissociation energy costs of 5.5 eV/H_2 and 8 eV/H_2, respectively. In another study, Marino et al. [95] used a DBD setup for encapsulating Cu and CuO particles with carbon. The authors demonstrated that increasing the residence time of Cu and CuO in the plasma region resulted in a higher carbon coverage proportion, even with a short treatment time. A DBD reactor was employed to synthesize g-C_3N_4, with surface-tailored vacancies, using melamine as a precursor. A potential of 10 kV was supplied by a plasma generator, where H_2 was employed as a carrier gas with a flow rate of 40 mL/min for 30 min. The plasma-treated catalyst was superior to thermally treated samples for H_2O_2 decomposition [96].

Guo et al. [97] reported that DBD plasma selectively produced monoclinic ZrO_2 by oxidizing the carbon template. Plasma exposure (DBD plasma at 14 kV, 22 kHz, and 250 W for 8 min) facilitated monoclinic ZrO_2 formation, which is thermally achieved through thermal calcination at temperatures above 1000 °C. In a similar study, the decomposition of carbonate during the synthesis of CuO-ZnO mixed oxide using a DBD setup was investigated. A potential of 20 kV was applied in the DBD reactor with 150 W input power. The plasma-assisted decomposition rate was about twice as fast as the thermal decomposition rate. Compared to the thermally prepared catalyst, the DBD plasma-treated CuO-ZnO catalyst exhibited a smaller particle size and higher Cu content (due to the decomposition of the precursor) on the catalyst surface. DRIFT analysis and activity tests showed that the DBD plasma-prepared CuO-ZnO catalyst displayed higher activity in the synthesis of methyl formate (MF) from syngas [98].

Wang et al. [99] used a DBD setup to reduce graphene oxide (GO). It was observed that upon plasma reduction with H_2 gas, the volume of the treated sample expanded several-fold compared to the untreated sample, as shown in Figure 23. This expansion was attributed to the exfoliation of GO sheets caused by the plasma treatment. These results were supported by BET surface area analysis, where the reduced sample exhibited a 20-fold increase in specific surface area compared to the untreated sample. The samples were tested for the hydrodesulfurization process, and the plasma-reduced sample demonstrated significantly higher activity than the untreated one. This enhanced activity was due to the high dispersion of metal nanoparticles, which significantly increased the surface area.

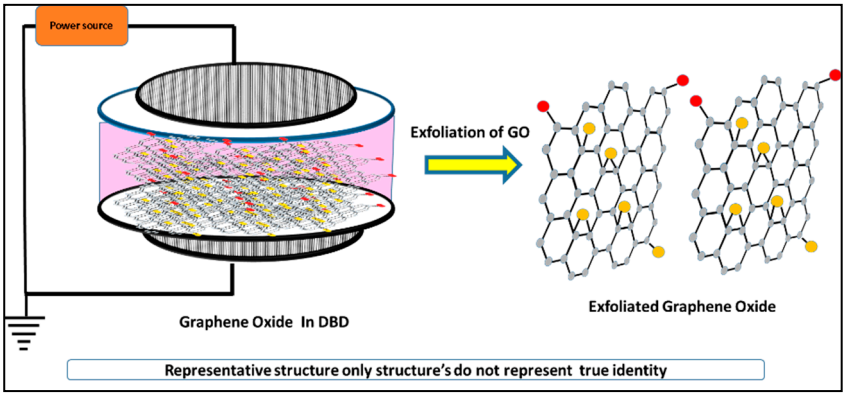

Figure 23. Application of DBD for the exfoliation of graphene oxide [99] (The red colour ball in the figure infers carboxylic acid group and yellow ball refers hydroxyl groups).

Li et al. [100] synthesized boron-doped GO by reducing a mixture of graphene oxide and boric acid. The prepared catalyst was reduced in DBD plasma for 3 min. H_2 was selected as the working gas because hydrogen radicals have a much higher reduction capability compared to molecular hydrogen and other gases (such as Ar and CO_2). The DBD plasma effectively breaks the Si-O-Si linkage, as observed in the case of SBA-15 silica [101]. When DBD plasma is applied in an oxygen medium, the Si-O-Si bond breaks to form Si-OH groups. Moreover, with increased irradiation time, the number of silanol hydroxyl groups rises. This modified SBA-15 silica was used to graft amine groups on its surface.

An efficient Pd Au/C catalyst was synthesized for formic acid dehydrogenation using a DBD reactor. The PdAu/C catalyst was placed in the DBD reactor, and plasma was ignited for 6 min with a 36 kV AC voltage (2 min each time) and 13.6 kHz frequency. The plasma-treated catalyst exhibited the highest catalytic activity, producing about 375 mL of the total gas (H_2 + CO) from formic acid decomposition, compared to 346 mL from the thermally calcined sample. The enhanced activity of the plasma-treated sample was attributed to smaller particle sizes of the active metal and an increased degree of alloying of the PdAu nanoparticles. Additionally, due to the columbic repulsion effect in plasma, more active metal sites were distributed on the outer surface of the support [102].

Bharti et al. [103] observed that the application of DBD treatment led to oxygen deficiencies and mixed oxidation states on Ti, specifically Ti^{+4} and Ti^{+3} states. The modifications were carried out under air plasma at a reduced pressure of 10^{-3} bar, with no change in the crystallinity of the samples after plasma ignition. Interestingly, the bandgap of TiO_2 increased after plasma treatment, likely due to increased charge separation between electrons and holes. Li et al. [104] used different gases in the DBD process to understand their influence on TiO_2 surface modification. Ti nanosheets with the (001) facet were treated with various gases, including Ar, H_2, and NH_3. The white TiO_2 (001) changed to a beige color in the Ar atmosphere due to oxygen vacancy generation. In contrast, the blue color of the TiO_2 in the H_2 treatment was attributed to the generation of Ti^{+3} on the TiO_2 surface. NH_3 treatment produced a yellow-green color, resulting from the synergistic effects of N doping and the presence of Ti^{+3} states, as shown in Figure 24a. UV studies supported these findings, with Ar-treated TiO_2 exhibiting absorption at wavelengths longer than 400 nm, indicating oxygen vacancy generation. Figure 24b shows the UV–visible absorption spectra for TiO_2 treated in various gas atmospheres. Interestingly, H_2-treated TiO_2 exhibited a tail extending into the infrared region, indicating the presence of Ti^{+3} states. NH_3-treated TiO_2 (001) nanosheets displayed an enlarged shoulder in the 400–550 nm range, corresponding to a bandgap of about 2.2 eV, likely due to nitrogen doping. XRD analysis revealed a peak shift to a higher diffraction angle, inflicting decreased inter-planner distance and the generation of vacancies.

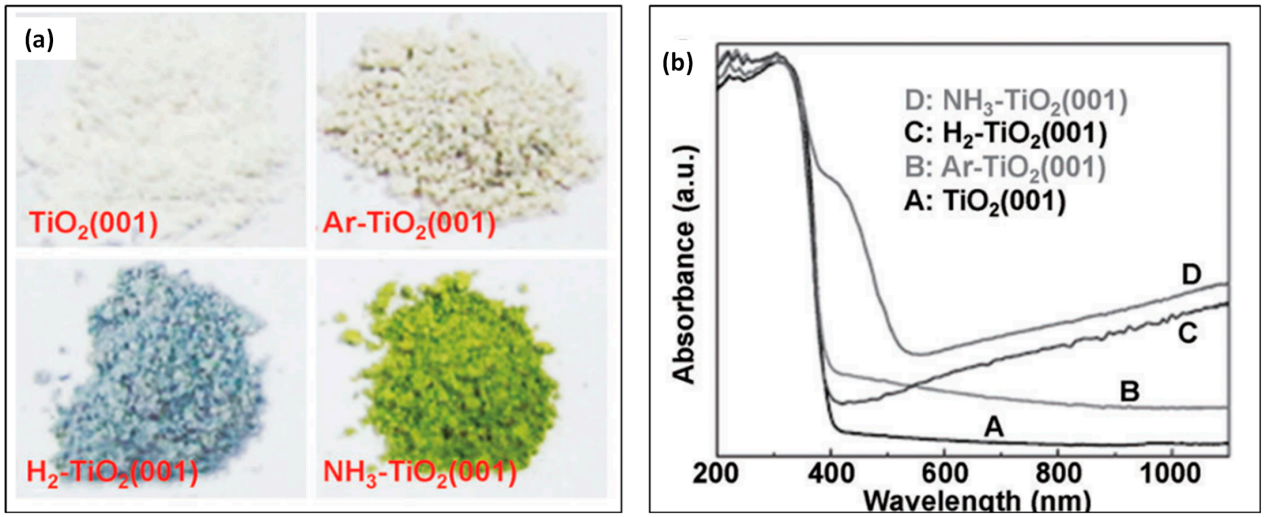

Figure 24. (**a**) Photographs of pristine TiO_2 (001) nanosheets (white) and modified samples; charge led to a structure difference. (**b**) UV–visible absorption spectra. Reproduced with permission from [104].

Similarly, solution-state CD plasma was applied for the synthesis of a defect-enriched TiO_2 photocatalyst by Yu et al. [105]. The authors found that plasma treatment in solution offered significant advantages over gas-phase plasma treatment, as no additional H_2 needed to be supplied. The schematic description is shown in Figure 25a. Instead, the H_2 generated from H_2O splitting could be utilized, allowing the process to be conducted at room temperature and atmospheric pressure, demonstrating its practicality. After plasma treatment, a shift in the absorption edge towards the visible region (around 700 nm) was observed, though, notably, there was no change in particle shape, size, and dispersion; structural and chemical composition; or surface area as seen from Figure 25b–d. A significant decrease in oxygen vacancies was observed, attributed to the high temperatures generated in the plasma zone. The shift in absorption edge towards visible light was due to an increase in Ti-OH bonds and the incorporation of hydrogen into the TiO_2 lattice at bridging sites. The plasma-treated catalyst was tested for the degradation of gaseous acetaldehyde and the reduction of CO_2 under UV light. It outperformed the untreated catalyst, delivering superior performance and stability in both applications.

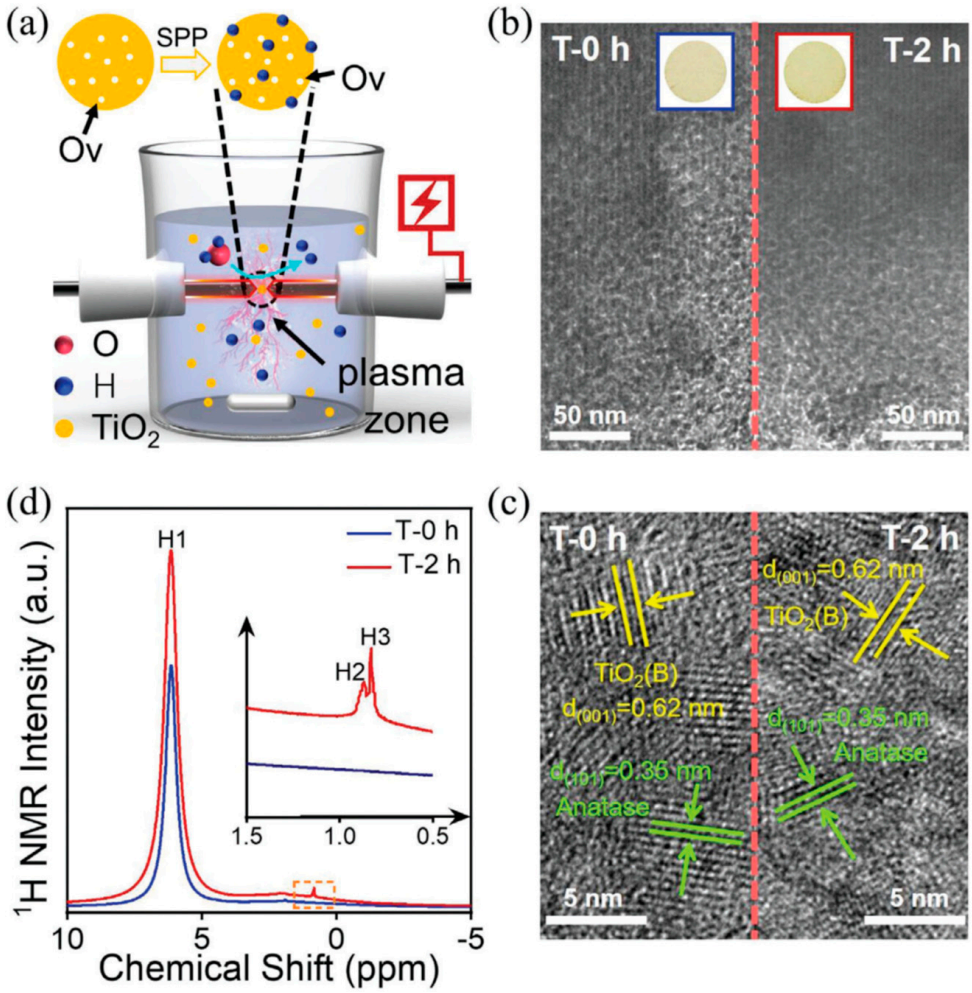

Figure 25. (**a**) Schematic of the SPP Technique. (**b**) TEM and (**c**) HRTEM images of TiO_2 treated by SPP for 0 and 2 h (samples T–0 h and T–2 h, respectively). (**d**) 1H NMR spectra of T–0 h and T-2 h, respectively. Reproduced with permission from [105].

The rapid advancements in the synthesis of nanomaterials (NMs) particularly emphasize innovative plasma generation techniques in liquid. One article discusses the unique properties of NMs and examines various types of plasma, such as arc and GD, that are used to produce a diverse array of materials, including metals, alloys, and composites. Additionally, the authors categorize existing experimental setups based on factors such as

the type of liquid used, electrode materials, configurations, and power sources, providing a comprehensive overview of the current research landscape in this field [106].

The surface oxygen vacancies and hydroxyl groups of a Al_2O_3 catalyst can be tuned by using different gas atmospheres. Plasma treatment of a Al_2O_3 catalyst with H_2 gas increased surface oxygen vacancies, whereas O_2 gas treatment led to a decrease in surface oxygen vacancies and an increase in surface hydroxyl groups. For the selective hydrogenation and dehydrogenation process, the presence of surface hydroxyl groups had a detrimental effect on the activity and stability of the catalyst. Surface hydroxyl groups facilitated H_2 spillover, reducing side reactions, thereby improving selectivity and product yield [107].

Plasma-treated CeO_2 showed a higher concentration of oxygen vacancies and Ce^{3+} (observed by XPS), a narrowed energy bandgap, and a 41.39% increase in specific surface area. These modifications in the plasma-treated catalyst enhanced the degradation of azophloxine in wastewater [108].

Liu et al. [109,110] used DBD plasma to oxidize the template cetyltrimethylammonium bromide while preparing MCM-41 molecular sieves. Air was used as the oxidizing medium, and two steel plates were separated by a quartz plate, as shown in Figure 23 (17 kV, 22 kHz). During the template oxidation, a change in color indicated the reaction of the template with the plasma, as seen in Figure 26. After prolonged plasma exposure of 75 min, the MCM-41 molecular sieve was free of the template, confirmed by the absence of C-H stretching in IR spectroscopy. Similarly, plasma treatment of ZSM-5 zeolite powder resulted in a dotted pattern, which the authors attributed to micro-discharges exhibiting two main characteristics: repetition and repulsion. Repulsion led to the self-organization of micro-discharges into regular structures [111].

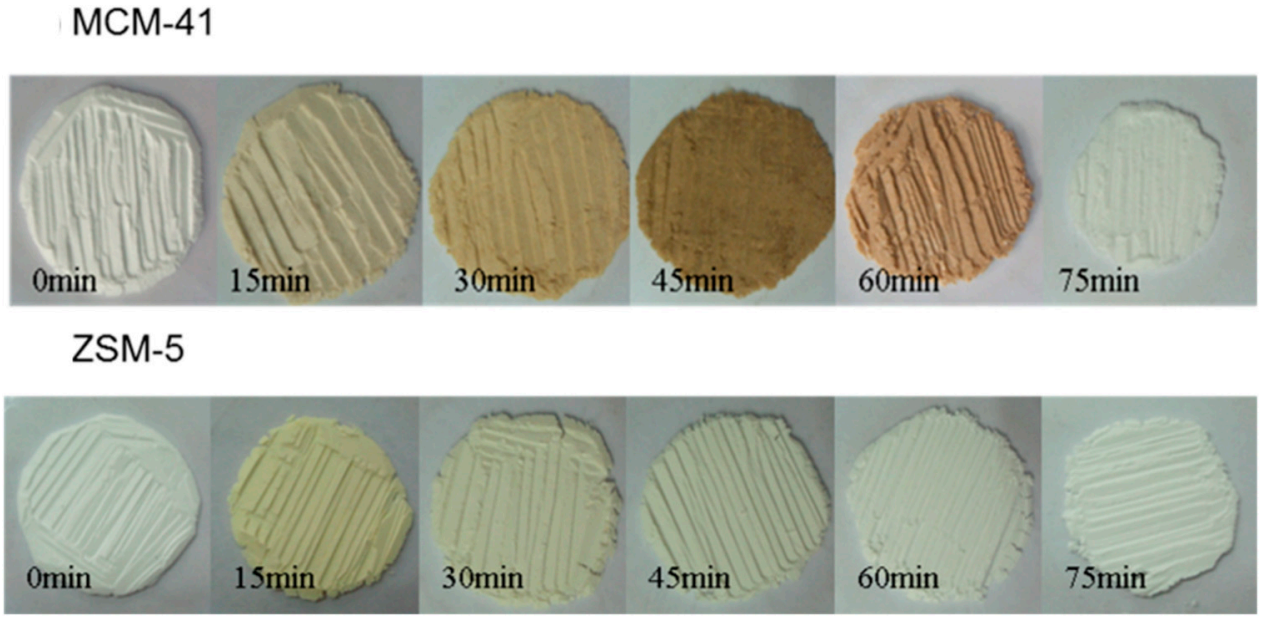

Figure 26. Color changes of the samples during DBD template removal. Reproduced with permission from [110].

The synthesis of low-coordinated Au atoms on TiO_2 was carried out using DBD plasma with O_2 at 2 W of input power. Plasma treatment altered the catalyst properties by decreasing particle size and promoting the formation of low-coordinated Au atoms on the TiO_2 support. Additionally, it introduced more surface hydroxyl groups compared to untreated samples [112]. The potential of plasma to improve surface functionalization by anchoring ester and carbonyl groups on fly ash was tested by Shi et al. [113] for Hg^0 removal from air.

GD plasma using Ar gas was applied to enhance oxygen vacancies and surface hydroxyl groups in a Cu_2O catalyst. The plasma-modified catalyst was used for the electrore-

duction of nitrates to NH_3, exhibiting superior performance compared to an untreated catalyst. This improvement was attributed to the increased oxygen vacancies and hydroxyl groups, which facilitated nitrate adsorption and proton transfer on the Cu_2O surface, leading to enhanced ammonia selectivity [114].

Plasma treatment has also been shown to improve crystallinity in samples, as demonstrated by Hájková and Tišler [115]. The DBD plasma, operated at 20 kV, 3 kHz, and 120 W of input power, produced a hydrotalcite-like structured catalyst. Remarkably, just 4 s of plasma irradiation resulted in better furfural conversion than the sample calcined at 450 °C for 6 h. The plasma treatment also induced sharp crystalline peaks in the XRD spectrum, which were absent in the calcined sample.

Nitrogen (N_2) doping of biomass-derived carbon was performed using a DBD reactor (3 kV, 10 kHz). The process occurred in a nitrogen (N_2) flow of 20 mL/min at room temperature and atmospheric pressure. The resulting biomass-derived carbon was applied in a pseudo capacitor, demonstrating a capacitance of 342.5 F/g at a current density of 0.5 A/g in 6 M KOH, along with excellent cyclic stability of 85.2% [116].

Ultrafine Pt nanoparticles were uniformly deposited on g-C_3N_4 through the plasma reduction of H_2PtCl_6, enabling precise control over the Pt size, composition, electronic structure, and interaction with g-C_3N_4 by adjusting the plasma discharge power. In addition, Ar plasma treatment introduced new oxygen-containing active groups on the g-C_3N_4 surface. The Ar-plasma-treated Pt/g-C_3N_4 composites demonstrated exceptional hydrogen evolution activity under visible light, achieving a hydrogen generation rate of 1150.8 μmol/h after 40 min of plasma treatment at 150 W. This rate was approximately 63.2 times higher than that of pristine g-C_3N_4 and 4.6 times higher than that of Pt/g-C_3N_4 composites produced using the photo deposition method [117].

Simultaneous N_2 doping and oxygen vacancy creation significantly enhanced oxygen evolution reactions (OERs), as observed by Liu et al. [118]. Oxygen vacancies and N doping not only improved the electronic structure of MnO_2, increasing its Mn^{3+} content to boost overall activity, but also stabilized Mn^{3+}, leading to remarkable long-term stability.

$MoSe_2$ nanosheets were created on a carbon film and modified using RF plasma (13.56 MHz, 10 to 40 W, 20 mT pressure, and 20 LPM Ar flow). This treatment significantly enhanced the hydrogen evolution reaction (HER) performance of the catalyst, achieving a lower overpotential of 148 mV at 10 mA cm^{-2} and a Tafel slope of 51.6 mV dec^{-1} after 20 W treatment.

The plasma treatment caused etching and increased oxygen vacancies, which improved H^+ adsorption and accelerated electron transfer by enhancing the electric field and active sites on the catalyst surface. The generated selenium (Se) vacancies increased the availability of molybdenum (Mo) atoms for H^+ reduction. Overall, this treatment boosted the catalyst's conductivity and H^+ absorption capacity, significantly enhancing HER performance [119].

Feng et al. [120] performed controlled nitrogen doping in MoS_2 nanosheets using RF plasma (PDC-002, Harrick, Pleasantville, NY, USA). The authors observed that plasma treatment significantly enhanced the surface wettability and affinity of N-doped MoS_2 compared to the pristine catalyst. This was evidenced by a notable reduction in contact angles, indicating better interaction with substrates. Nitrogen doping via plasma treatment led to the formation of Mo−N bonds, which not only stabilized the doped nitrogen but also contributed to the overall stability and efficiency of the catalyst in aqueous environments. Additionally, N-doped MoS_2 exhibited a lower Fermi level compared to pristine MoS_2, facilitating improved electron transfer during catalytic reactions, thus enhancing its overall catalytic performance, especially for mimicking peroxidase-like enzymes.

Liu et al. [121] generated oxygen vacancies in Mn/ZSM-5 catalysts for VOC abatement (methanol, acetone, and toluene) using three distinct methods: steaming, doping, and plasma treatment. Using the tested methods, the oxygen vacancy generation was 33.1%, 51.3%, and 53.7% for steaming, doping, and plasma, respectively. Furthermore, the specific surface area of Mn/ZSM-5 decreased from 424 m^2/g to 363, 370, and 402 m^2/g for the

steaming, doping, and plasma methods, respectively. A similar trend was observed for microporous surface area. The decrease in surface area for the steaming method was attributed to high-temperature conditions that could collapse the pores. For the doping method, pore blockage occurred due to the addition of external dopants, while plasma, being a physical method, initiated surface modification under milder conditions without introducing heterogeneous dopant materials. These factors contributed to the superior behavior of the plasma-generated oxygen vacancies in VOC abatement.

In addition to surface modifications, plasma treatment has been shown to enhance the magnetic properties of ferrites. Mohan et al. [122] synthesized inverse spinels of $CoFe_2O_4$ using DBD-assisted plasma treatment for 30 min at 200 °C. The plasma-treated material exhibited superior magnetic properties, with a magnetization (Ms) of 91.80 emu/g and coercivity (Hc) of 888 Oe, demonstrating the effectiveness of plasma treatment in enhancing magnetic properties.

In most studies, the beneficial role of plasma treatment in enhancing catalyst performance is emphasized. However, plasma also negatively affects catalysts. For instance, Yi et al. [123] investigated the catalytic combustion of C_2H_6 at equivalence ratios of 1.0 and 1.4 over NTP-modified Pd/Al_2O_3. The authors compared the activity of untreated Pd/Al_2O_3 with plasma-modified Pd/Al_2O_3 and found that the catalyst activation temperatures shifted to higher values by approximately 30–50 °C for plasma-treated catalysts. Furthermore, significantly more CO was formed in the C_2H_6 combustion at higher temperatures for the plasma-modified catalysts. The authors attributed the decrease in activity to the reduction in surface area caused by plasma treatment, which led to decreased catalytic activity. Additionally, the leaching of Pd species and the transformation of γ-Al_2O_3 to θ-Al_2O_3 were observed after the NTP treatment due to the impact of highly energetic electrons.

Several researchers have evaluated the potential of different NTPs for cleaning surfaces and enhancing catalyst performance enhancers. Zhang et al. [124] treated Mo-Ni sulfide/γ-Al_2O_3 and Mo-Co oxide/γ-Al_2O_3 catalysts in ambient air using RF plasma jet, DBD, and spark discharge. The surface morphology, chemical states, and functional groups of the catalysts were significantly altered after treatment with NTPs, as evidenced by surface analysis. Compared to the untreated catalyst, the surface became smoother after RF plasma jet treatment but rougher after DBD or spark discharge treatment. This variation was due to the primary agents involved: heavy particles (Ar metastable states) in the RF plasma jet, high-energy electrons in the DBD, and heat in the spark discharge. Notably, the oxidation states of Mo were enhanced following DBD treatment through interaction with oxygen atoms, suggesting that DBD could be an effective tool for controlling Mo oxidation states. Additionally, the Raman spectrum of MoS_2 disappeared after RF plasma jet treatment, indicating significant destruction of the MoS_2 layers in the Mo-Ni sulfide/γ-Al_2O_3 catalyst.

5. Overall Perspectives of Catalyst Synthesis/Modification by Cold Plasma

This review has demonstrated the benefits of plasma technology for various processes, including reduction, oxidation, template removal, and material synthesis. Four different types of NTPs and their respective roles were discussed in detail. Moreover, the plasma-synthesized or -engineered materials were compared with those produced through conventional methods such as thermal heating. Plasma treatment enhances catalytic activity by inducing modifications under different gas atmospheres. These modifications can include changes in the catalyst oxidation state, redistribution of acidic and basic sites, improved metal dispersion, and other alterations, as illustrated in Figure 27.

The altered chemical and physical properties of plasma-treated catalysts have been effectively utilized for GHG mitigation. Various mitigation techniques are highlighted, including the production of value-added products like syngas, alcohols, hydrocarbons, and more, from GHGs. The strategies presented in this review offer a pathway towards closed-loop GHG mitigation, helping to reduce carbon emissions and lower our carbon footprint.

s

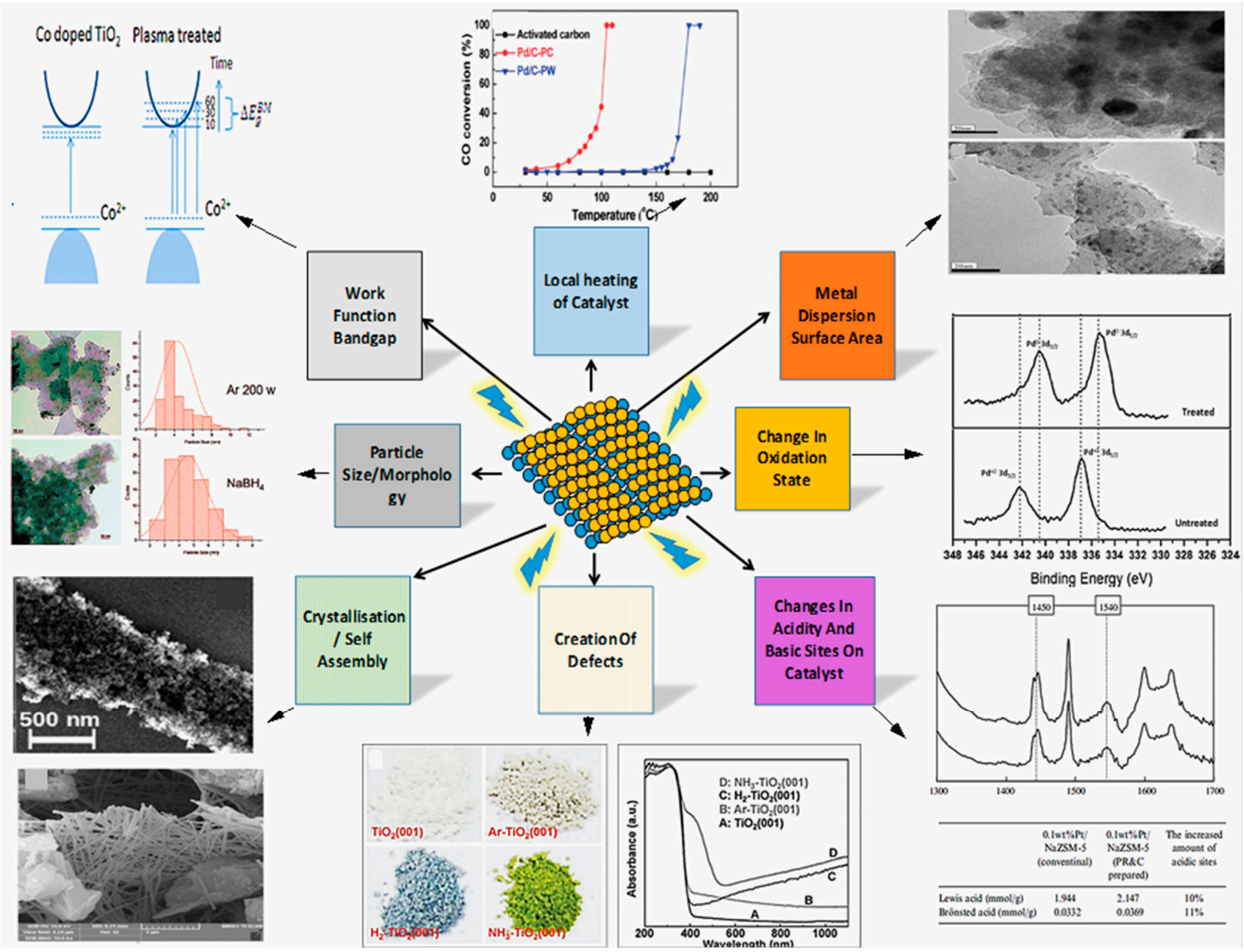

Figure 27. Impacts of plasma treatment on catalyst physicochemical properties.

Plasma-induced modification significantly enhances catalytic activity by lowering the activation energy and improving conversion rates and product yields. Remarkably, even a short plasma treatment duration is sufficient to induce irreversible changes that remain stable, even after subsequent high-temperature calcining. Furthermore, plasma treatment can be applied at various stages of catalyst preparation, effectively altering reaction dynamics and catalytic properties. Importantly, plasma technology reduces energy consumption by eliminating the need for prolonged heating typically required in calcination and thermal catalysis. This makes plasma treatment a more energy-efficient and environmentally friendly approach to material synthesis.

6. Conclusions

In this review, we attempted to showcase the diversified types of cold plasmas and their application for catalyst synthesis and surface modifications. Extensive literature was presented to showcase the conversion of GHGs into a variety of products, namely, synthesis gas, alcohols, and others, by using a conventional catalyst and plasma-treated catalyst. The high electron temperatures in a cold plasma act as a key factor for different applications. Cold plasmas are most commonly employed for the reduction of metallic substrates. The reducibility of metallic precursors depends upon the standard reduction potential of M^{n+}/M^0 pairs.

Cold plasma has several added advantages over conventional processes:

(1) Cold plasma operates at low temperatures, which makes it suitable for temperature-sensitive substrates.

(2) Since cold plasmas are non-equilibrium plasmas, they generate electrons and ions in a plasma plume. These electrons can actively take part in reduction processes without the need for an additional reducing agent.

(3) The short plasma treatment time can bring desired changes that otherwise require a long treatment time and harsh gaseous atmosphere.

(4) The plasma treatment leads to smaller particle sizes of active catalyst material, and higher dispersion is observed due to Coloumbic repulsive forces acting on particles suspended on supports.

(5) Catalytic properties are boosted due to high metal-to-support interactions.

These advantages make cold plasma treatment more desirable than other methods. However, the application of plasma is a new area of research, although there have been an increasing number of publications and patents on this topic. In low-temperature operation, the residues from plasma decomposition or plasma reduction remain on the catalyst support. Part of the undecomposed precursors may cause distortions of the structure generated by the plasma. If moisture is present, a specific catalyst precursor hydrate may be observed. Therefore, in many cases, thermal treatment or washing must be performed after the plasma operation. Since the plasma application for catalyst synthesis is an emerging research area, the understanding of plasma physics and plasma chemistry associated with equilibrium thermodynamics is important and needs to be evaluated. There are no tools to measure the electron density and energy and other active or intermediate species during catalyst preparation. Additionally, it is unclear which parameter plays a crucial role in catalyst synthesis. Moreover, the absence of in situ characterizations during plasma operation limits the understanding of the plasma–catalyst interaction. However, with the growing interest of the scientific community and technological advances, more insights will be discovered in the upcoming years.

The primary drawback of NTP systems is their limited processing capacity, which can make them less suitable for large-scale industrial applications, as this constraint affects their ability to efficiently handle substantial amounts of materials or contaminants. Additionally, while NTP technologies are generally more energy-efficient than thermal alternatives, excessive energy consumption remains a concern, especially when scaling operations. Optimizing energy utilization is, therefore, essential to improve the feasibility of NTP approaches for broader applications.

Another significant challenge is the creation of byproducts during NTP processes, which can complicate subsequent purification efforts and pose environmental concerns. The range of materials treatable by NTP is also limited; not all compounds are suitable for NTP treatment as some may degrade or experience unwanted changes under plasma conditions. Achieving precise control over plasma characteristics—such as temperature, electron density, and reactive species concentration—is crucial but challenging for reliable material synthesis.

Maintaining stable plasma discharge is necessary for effective processing as variations in discharge stability can significantly impact the quality and consistency of synthesis outcomes. Accurate measurements of plasma properties, including electron temperature and density, are especially difficult in atmospheric-pressure plasmas, further complicating process optimization. In catalyst applications, interactions between plasma and catalyst materials can alter expected outcomes, adding complexity to achieving the desired catalytic performance. Moreover, compliance with safety and environmental regulations poses additional challenges to the deployment of NTP technology.

Finally, there remain many open questions regarding the fundamental mechanisms driving NTP processes, making it difficult to develop optimized material synthesis methods. Addressing these limitations and challenges is essential for the advancement and broader adoption of non-thermal plasma technologies across various industries.

Author Contributions: Conceptualization, N.J. and S.L.; writing—original draft preparation, N.J.; writing—review and editing, S.L. All authors have read and agreed to the published version of the manuscript.

Funding: This research received no external funding.

Data Availability Statement: Data are available in a publicly accessible repository.

Conflicts of Interest: The authors declare no conflicts of interest.

References

1. McNaught, A.D.; Wilkinson, A. *Compendium of Chemical Terminology*; Blackwell Science Oxford: Oxford, UK, 1997; Volume 1669.
2. Hutchings, G.J. Catalyst synthesis using supercritical carbon dioxide: A green route to high activity materials. *Top. Catal.* **2009**, *52*, 982–987. [CrossRef]
3. Yang, X.; Liu, Y.; Li, J.; Zhang, Y. Effects of calcination temperature on morphology and structure of CeO_2 nanofibers and their photocatalytic activity. *Mater. Lett.* **2019**, *241*, 76–79. [CrossRef]
4. Bogaerts, A.; Neyts, E.; Gijbels, R.; Van der Mullen, J. Gas discharge plasmas and their applications. *J. Spectrochim. Acta Part B At. Spectrosc.* **2002**, *57*, 609–658. [CrossRef]
5. Fridman, A. *Plasma Chemistry*; Cambridge University Press: Cambridge, UK, 2008.
6. Mizuno, A. Recent progress and applications of non-thermal plasma. *Int. J. Plasma Environ. Sci. Technol.* **2009**, *3*, 1–7.
7. Mizuno, A.; Fusion, C. Industrial applications of atmospheric non-thermal plasma in environmental remediation. *Plasma Phys. Control. Fusion* **2007**, *49*, A1. [CrossRef]
8. Moreau, M.; Orange, N.; Feuilloley, M. Non-thermal plasma technologies: New tools for bio-decontamination. *Biotechnol. Adv.* **2008**, *26*, 610–617. [CrossRef]
9. Mumtaz, S.; Khan, R.; Rana, J.N.; Javed, R.; Iqbal, M.; Choi, E.H.; Han, I. Review on the biomedical and environmental applications of nonthermal plasma. *Catalysts* **2023**, *13*, 685. [CrossRef]
10. Guo, L.; Yan, M.; Gong, H.; Zou, Z.; Henningsen, A. Application of non-thermal plasma in medicine: A bibliometric and visualization analysis. *Front. Phys.* **2023**, *11*, 1325851. [CrossRef]
11. Vollath, D. Plasma synthesis of nanoparticles. *KONA Powder* **2007**, *25*, 39–55. [CrossRef]
12. Sundgren, J.-E. Physics of Glow Discharge Plasmas and Plasma/Surface Interactions During Thin Film Growth. In *Diamond and Diamond-like Films and Coatings*; Springer: Berlin/Heidelberg, Germany, 1991; pp. 47–71.
13. Eliasson, B.; Kogelschatz, U. Nonequilibrium volume plasma chemical processing. *IEEE Trans. Plasma Sci.* **1991**, *19*, 1063–1077. [CrossRef]
14. Tyczkowski, J.; Kapica, R. Cold plasma in the nanotechnology of catalysts. *Pol. J. Chem. Technol.* **2007**, *9*, 36–42. [CrossRef]
15. Witvrouwen, T.; Paulussen, S.; Sels, B. The Use of Non-Equilibrium Plasmas for the Synthesis of Heterogeneous Catalysts. *Plasma Process. Polym.* **2012**, *9*, 750–760. [CrossRef]
16. Wang, Z.; Zhang, Y.; Neyts, E.C.; Cao, X.; Zhang, X.; Jang, B.W.-L.; Liu, C.-J. Catalyst preparation with plasmas: How does it work? *ACS Catal.* **2018**, *8*, 2093–2110. [CrossRef]
17. Taghvaei, H.; Heravi, M.; Rahimpour, M.R. Synthesis of supported nanocatalysts via novel non-thermal plasma methods and its application in catalytic processes. *Plasma Process. Polym.* **2017**, *14*, 1600204. [CrossRef]
18. Kortshagen, U.R.; Sankaran, R.M.; Pereira, R.N.; Girshick, S.L.; Wu, J.J.; Aydil, E.S. Nonthermal plasma synthesis of nanocrystals: Fundamental principles, materials, and applications. *Chem. Rev.* **2016**, *116*, 11061–11127. [CrossRef]
19. Khoja, A.H.; Mazhar, A.; Saleem, F.; Mehran, M.T.; Naqvi, S.R.; Anwar, M.; Shakir, S.; Amin, N.A.S.; Sajid, M.B. Recent developments in catalyst synthesis using DBD plasma for reforming applications. *Int. J. Hydrogen Energy* **2021**, *46*, 15367–15388. [CrossRef]
20. Liu, C.-J.; Vissokov, G.P.; Jang, B.W.-L. Catalyst preparation using plasma technologies. *Catal. Today* **2002**, *72*, 173–184. [CrossRef]
21. Santos, A.M.d.; Catapan, R.C.; Duarte, D.A. The potential of non-thermal plasmas in the preparation of supported metal catalysts for fuel conversion in automotive systems: A literature overview. *Front. Mech. Eng.* **2020**, *6*, 42. [CrossRef]
22. Liu, C.-J.; Zou, J.; Yu, K.; Cheng, D.; Han, Y.; Zhan, J.; Ratanatawanate, C.; Jang, B.W.-L. Plasma application for more environmentally friendly catalyst preparation. *Pure Appl. Chem.* **2006**, *78*, 1227–1238. [CrossRef]
23. Ye, Z.; Zhao, L.; Nikiforov, A.; Giraudon, J.-M.; Chen, Y.; Wang, J.; Tu, X. A review of the advances in catalyst modification using nonthermal plasma: Process, Mechanism and Applications. *Adv. Colloid Interface Sci.* **2022**, *308*, 102755. [CrossRef]
24. Di, L.; Zhang, J.; Zhang, X.; Wang, H.; Li, H.; Li, Y.; Bu, D. Cold plasma treatment of catalytic materials: A review. *J. Phys. D Appl. Phys.* **2021**, *54*, 333001. [CrossRef]
25. Zhang, L.; Liu, X.; Scurrell, M.S. Cold plasmas in the modification of catalysts. *Rev. Chem. Eng.* **2018**, *34*, 201–213. [CrossRef]
26. Di, L.; Zhang, J.; Zhang, X. A review on the recent progress, challenges, and perspectives of atmospheric-pressure cold plasma for preparation of supported metal catalysts. *Plasma Process. Polym.* **2018**, *15*, 1700234. [CrossRef]
27. Tyczkowski, J. Cold plasma produced catalytic materials. In *Plasma Science Technology—Progress in Physical States Chemical Reactions*; InTech: Rijeka, Croatia, 2016; pp. 53–93.
28. Stevens, J. *Plasma Fundamentals for Materials Processing*; Springer: Berlin/Heidelberg, Germany, 2000; pp. 33–68.

29. McDaniel, E.W.; Mitchell, J.; Rudd, M.E. *Atomic Collisions: Heavy-Particle Projectiles*; U.S. Department of Energy Office of Scientific and Technical Information: Oak Ridge, TN, USA, 1993.
30. Yu, X.; Zhang, F.; Wang, N.; Hao, S.; Chu, W. Plasma-treated bimetallic Ni–Pt catalysts derived from hydrotalcites for the carbon dioxide reforming of methane. *Catal. Lett.* **2014**, *144*, 293–300. [CrossRef]
31. Wang, N.; Shen, K.; Yu, X.; Qian, W.; Chu, W. Preparation and characterization of a plasma treated NiMgSBA-15 catalyst for methane reforming with CO_2 to produce syngas. *Catal. Sci. Technol.* **2013**, *3*, 2278–2287. [CrossRef]
32. Rahemi, N.; Haghighi, M.; Babaluo, A.A.; Jafari, M.F.; Estifaee, P. Synthesis and physicochemical characterizations of Ni/Al_2O_3–ZrO_2 nanocatalyst prepared via impregnation method and treated with non-thermal plasma for CO_2 reforming of CH_4. *J. Ind. Eng. Chem.* **2013**, *19*, 1566–1576. [CrossRef]
33. Pan, Y.-X.; Liu, C.-J.; Shi, P. Preparation and characterization of coke resistant Ni/SiO_2 catalyst for carbon dioxide reforming of methane. *J. Power Sources* **2008**, *176*, 46–53. [CrossRef]
34. Cheng, D.-G.; Zhu, X.; Ben, Y.; He, F.; Cui, L.; Liu, C.-J. Carbon dioxide reforming of methane over Ni/Al_2O_3 treated with glow discharge plasma. *Catal. Today* **2006**, *115*, 205–210. [CrossRef]
35. Zhao, Y.; Pan, Y.-X.; Xie, Y.; Liu, C.-J. Carbon dioxide reforming of methane over glow discharge plasma-reduced Ir/Al_2O_3 catalyst. *Catal. Commun.* **2008**, *9*, 1558–1562. [CrossRef]
36. Liu, C.-J.; Cheng, D.-G.; Zhang, Y.-P.; Yu, K.-L.; Xia, Q.; Wang, J.-G.; Zhu, X.-L. Remarkable enhancement in the dispersion and low-temperature activity of catalysts prepared via novel plasma reduction-calcination method. *Catal. Surv. Asia* **2004**, *8*, 111–118. [CrossRef]
37. Karuppiah, J.; Mok, Y.S. Plasma-reduced Ni/γ–Al_2O_3 and CeO_2–Ni/γ–Al_2O_3 catalysts for improving dry reforming of propane. *Int. J. Hydrogen Energy* **2014**, *39*, 16329–16338. [CrossRef]
38. Jin, L.; Li, Y.; Lin, P.; Hu, H. CO_2 reforming of methane on Ni/γ-Al_2O_3 catalyst prepared by dielectric barrier discharge hydrogen plasma. *Int. J. Hydrogen Energy* **2014**, *39*, 5756–5763. [CrossRef]
39. Hua, W.; Jin, L.; He, X.; Liu, J.; Hu, H. Preparation of Ni/MgO catalyst for CO_2 reforming of methane by dielectric-barrier discharge plasma. *Catal. Commun.* **2010**, *11*, 968–972. [CrossRef]
40. Fang, X.; Lian, J.; Nie, K.; Zhang, X.; Dai, Y.; Xu, X.; Wang, X.; Liu, W.; Li, C.; Zhou, W. Dry reforming of methane on active and coke resistant $Ni/Y_2Zr_2O_7$ catalysts treated by dielectric barrier discharge plasma. *J. Energy Chem.* **2016**, *25*, 825–831. [CrossRef]
41. Zhang, H.; Chu, W.; Xu, H.; Zhou, J. Plasma-assisted preparation of Fe–Cu bimetal catalyst for higher alcohols synthesis from carbon monoxide hydrogenation. *Fuel* **2010**, *89*, 3127–3131. [CrossRef]
42. Chen, M.; Chu, W.; Dai, X.; Zhang, X. New palladium catalysts prepared by glow discharge plasma for the selective hydrogenation of acetylene. *Catal. Today* **2004**, *89*, 201–204. [CrossRef]
43. Bian, L.; Zhang, L.; Xia, R.; Li, Z. Enhanced low-temperature CO_2 methanation activity on plasma-prepared Ni-based catalyst. *J. Nat. Gas Sci. Eng.* **2015**, *27*, 1189–1194. [CrossRef]
44. Tu, X.; Gallon, H.; Whitehead, J. Plasma-assisted reduction of a NiO/Al_2O_3 catalyst in atmospheric pressure H_2/Ar dielectric barrier discharge. *Catal. Today* **2013**, *211*, 120–125. [CrossRef]
45. Benrabbah, R.; Cavaniol, C.; Liu, H.; Ognier, S.; Cavadias, S.; Gálvez, M.E.; Da Costa, P. Plasma DBD activated ceria-zirconia-promoted Ni-catalysts for plasma catalytic CO_2 hydrogenation at low temperature. *J. Catal. Commun.* **2017**, *89*, 73–76. [CrossRef]
46. Fan, Z.; Sun, K.; Rui, N.; Zhao, B.; Liu, C.-J. Improved activity of $Ni/MgAl_2O_4$ for CO_2 methanation by the plasma decomposition. *J. Energy Chem.* **2015**, *24*, 655–659. [CrossRef]
47. Zhao, B.; Chen, Z.; Chen, Y.; Ma, X. Syngas methanation over Ni/SiO_2 catalyst prepared by ammonia-assisted impregnation. *Int. J. Hydrogen Energy* **2017**, *42*, 27073–27083. [CrossRef]
48. Kim, S.-S.; Lee, H.; Na, B.-K.; Song, H.K. Plasma-assisted reduction of supported metal catalyst using atmospheric dielectric-barrier discharge. *Catal. Today* **2004**, *89*, 193–200. [CrossRef]
49. Joshi, N.; Loganathan, S. In situ modification of CuO–Fe_2O_3 by nonthermal plasma: Insights into the CO_2-to-CH_3OH hydrogenation reaction. *ACS Omega* **2023**, *8*, 13410–13420. [CrossRef] [PubMed]
50. Joshi, N.; Loganathan, S. Methanol synthesis from CO_2 using Ni and Cu supported Fe catalytic system: Understanding the role of nonthermal plasma surface discharge. *Plasma Process. Polym.* **2021**, *18*, 2000104. [CrossRef]
51. Joshi, N.; Sivachandiran, L. Exploring the feasibility of liquid fuel synthesis from CO_2 under cold plasma discharge: Role of plasma discharge in binary metal oxide surface modification. *RSC Adv.* **2021**, *11*, 27757–27766. [CrossRef]
52. Zhang, S.; Chen, C.-Y.; Jang, B.W.-L.; Zhu, A.-M. Radio-frequency H_2 plasma treatment of $AuPd/TiO_2$ catalyst for selective hydrogenation of acetylene in excess ethylene. *Catal. Today* **2015**, *256*, 161–169. [CrossRef]
53. Li, Y.; Jang, B.W. Non-thermal RF plasma effects on surface properties of Pd/TiO_2 catalysts for selective hydrogenation of acetylene. *Appl. Catal. A Gen.* **2011**, *392*, 173–179. [CrossRef]
54. Zhang, M.; Li, P.; Zhu, M.; Tian, Z.; Dan, J.; Li, J.; Dai, B.; Yu, F. Ultralow-weight loading Ni catalyst supported on two-dimensional vermiculite for carbon monoxide methanation. *Chin. J. Chem. Eng.* **2018**, *26*, 1873–1878. [CrossRef]
55. Jia, X.; Rui, N.; Zhang, X.; Hu, X.; Liu, C.-J. Ni/ZrO_2 by dielectric barrier discharge plasma decomposition with improved activity and enhanced coke resistance for CO methanation. *Catal. Today* **2019**, *334*, 215–222. [CrossRef]
56. Chen, H.; Mu, Y.; Shao, Y.; Chansai, S.; Xiang, H.; Jiao, Y.; Hardacre, C.; Fan, X. Nonthermal plasma (NTP) activated metal–organic frameworks (MOFs) catalyst for catalytic CO_2 hydrogenation. *AIChE J.* **2020**, *66*, e16853. [CrossRef]

57. Yu, J.; Feng, B.; Liu, S.; Mu, X.; Lester, E.; Wu, T. Highly active Ni/Al_2O_3 catalyst for CO_2 methanation by the decomposition of Ni-MOF@ Al_2O_3 precursor via cold plasma. *Appl. Energy* **2022**, *315*, 119036. [CrossRef]
58. Ul Haq, A.; Fanelli, F.; Bekris, L.; Martin, A.M.; Lee, S.; Khalid, H.; Savaniu, C.D.; Kousi, K.; Metcalfe, I.S.; Irvine, J.T. Dielectric barrier plasma discharge exsolution of nanoparticles at room temperature and atmospheric pressure. *Adv. Sci.* **2024**, *11*, 2402235. [CrossRef] [PubMed]
59. Zhang, Y.; Chu, W.; Cao, W.; Luo, C.; Wen, X.; Zhou, K. A plasma-activated Ni/α-Al_2O_3 catalyst for the conversion of CH_4 to syngas. *Plasma Chem. Plasma Process.* **2000**, *20*, 137–144. [CrossRef]
60. Nugraha, H.; Imaduddin, A.; Wismogroho, A.S. Analysis of Required Electric Power in Tube Furnace Using DAQ master Program. In Proceedings of the IRSTC ISTN International Seminar 2015, Aceh, Indonesia, 18–20 November 2015.
61. Nazarpoor, Z.; Ma, S.; Fanson, P.T.; Alexeev, O.S.; Amiridis, M.D. O_2 plasma activation of dendrimer-derived Pt/γ-Al_2O_3 catalysts. *J. Catal.* **2012**, *290*, 26–36. [CrossRef]
62. Li, Z.-H.; Tian, S.-X.; Wang, H.-T.; Tian, H.-B. Plasma treatment of Ni catalyst via a corona discharge. *J. Mol. Catal. A Chem.* **2004**, *211*, 149–153. [CrossRef]
63. Wang, J.-G.; Liu, C.-J.; Zhang, Y.-P.; Yu, K.-L.; Zhu, X.-L.; He, F. Partial oxidation of methane to syngas over glow discharge plasma treated Ni–Fe/Al_2O_3 catalyst. *Catal. Today* **2004**, *89*, 183–191. [CrossRef]
64. Chen, M.-H.; Chu, W.; Zhu, J.-J.; Dong, L. Plasma assisted preparation of cobalt catalysts by sol–gel method for methane combustion. *J. Sol-Gel Sci. Technol.* **2008**, *47*, 354–359. [CrossRef]
65. Qi, B.; Di, L.; Xu, W.; Zhang, X. Dry plasma reduction to prepare a high performance Pd/C catalyst at atmospheric pressure for CO oxidation. *J. Mater. Chem. A* **2014**, *2*, 11885–11890. [CrossRef]
66. Di, L.; Li, Z.; Lee, B.; Park, D.-W. An alternative atmospheric-pressure cold plasma method for synthesizing Pd/P25 catalysts with the assistance of ethanol. *Int. J. Hydrogen Energy* **2017**, *42*, 11372–11378. [CrossRef]
67. Di, L.; Zhan, Z.; Zhang, X.; Qi, B.; Xu, W. Atmospheric-pressure DBD cold plasma for preparation of high active Au/P25 catalysts for low-temperature CO oxidation. *Plasma Sci. Technol.* **2016**, *18*, 544. [CrossRef]
68. Cheng, D.-G. Plasma decomposition and reduction in supported metal catalyst preparation. *Catal. Surv. Asia* **2008**, *12*, 145–151. [CrossRef]
69. Cheng, D.-G.; Zhu, X. Reduction of Pd/HZSM-5 using oxygen glow discharge plasma for a highly durable catalyst preparation. *Catal. Lett.* **2007**, *118*, 260–263. [CrossRef]
70. Huang, L.; Chu, W.; Zhang, T.; Yin, Y.; Tao, X. Preparation of novel Ni-Ir/γ-Al_2O_3 catalyst via high-frequency cold plasma direct reduction process. *J. Nat. Gas Chem.* **2009**, *18*, 35–38. [CrossRef]
71. Buitrago-Sierra, R.; García-Fernández, M.J.; Pastor-Blas, M.M.; Sepúlveda-Escribano, A. Environmentally friendly reduction of a platinum catalyst precursor supported on polypyrrole. *Green Chem.* **2013**, *15*, 1981–1990. [CrossRef]
72. Pelalak, R.; Alizadeh, R.; Ghareshabani, E. Enhanced heterogeneous catalytic ozonation of pharmaceutical pollutants using a novel nanostructure of iron-based mineral prepared via plasma technology: A comparative study. *J. Hazard. Mater.* **2020**, *392*, 122269. [CrossRef]
73. Roy, B.; Loganathan, K.; Pham, H.; Datye, A.; Leclerc, C. Surface modification of solution combustion synthesized Ni/Al_2O_3 catalyst for aqueous-phase reforming of ethanol. *Int. J. Hydrogen Energy* **2010**, *35*, 11700–11708. [CrossRef]
74. Kameoka, S.; Kuroda, M.; Ito, S.-I.; Kunimori, K. Fomation of a novel Al_2O_3 surface (Al–O*) by plasma-excited nitrogen: O_2 production by water treatment of the Al–O* surface. *Chem. Commun.* **1996**, *18*, 2215–2216. [CrossRef]
75. Liu, Y.; Bai, X. Argon glow discharge plasma-reduced palladium nanoparticles supported on activated carbon for Suzuki and Heck coupling reactions. *Appl. Organomet. Chem.* **2017**, *31*, e3561. [CrossRef]
76. Li, Z.; Meng, J.; Wang, W.; Wang, Z.; Li, M.; Chen, T.; Liu, C.-J. The room temperature electron reduction for the preparation of silver nanoparticles on cotton with high antimicrobial activity. *Carbohydr. Polym.* **2017**, *161*, 270–276. [CrossRef]
77. Wang, Z.-J.; Xie, Y.; Liu, C.-J. Synthesis and characterization of noble metal (Pd, Pt, Au, Ag) nanostructured materials confined in the channels of mesoporous SBA-15. *J. Phys. Chem. C* **2008**, *112*, 19818–19824. [CrossRef]
78. Shang, S.; Liu, G.; Chai, X.; Tao, X.; Li, X.; Bai, M.; Chu, W.; Dai, X.; Zhao, Y.; Yin, Y. Research on Ni/γ-Al_2O_3 catalyst for CO_2 reforming of CH_4 prepared by atmospheric pressure glow discharge plasma jet. *Catal. Today* **2009**, *148*, 268–274. [CrossRef]
79. Bogaerts, A.; Tu, X.; Whitehead, J.C.; Centi, G.; Lefferts, L.; Guaitella, O.; Azzolina-Jury, F.; Kim, H.-H.; Murphy, A.B.; Schneider, W.F. The 2020 plasma catalysis roadmap. *J. Phys. D Appl. Phys.* **2020**, *53*, 443001. [CrossRef]
80. Zou, J.-J.; Liu, C.-J.; Zhang, Y.-P. Control of the metal− support interface of NiO-loaded photocatalysts via cold plasma treatment. *Langmuir* **2006**, *22*, 2334–2339. [CrossRef]
81. Chen, Y.; Wang, H.; Liu, C.-J.; Zeng, Z.; Zhang, H.; Zhou, C.; Jia, X.; Yang, Y. Formation of monometallic Au and Pd and bimetallic Au–Pd nanoparticles confined in mesopores via Ar glow-discharge plasma reduction and their catalytic applications in aerobic oxidation of benzyl alcohol. *J. Catal.* **2012**, *289*, 105–117. [CrossRef]
82. Yu, K.-L.; Zou, J.-J.; Ben, Y.-H.; Zhang, Y.-P.; Liu, C.-J. Synthesis of NiO-embedded carbon nanotubes using corona discharge enhanced chemical vapor deposition. *Diam. Relat. Mater.* **2006**, *15*, 1217–1222. [CrossRef]
83. Li, M.; Hu, Z.; Wang, X.; Wu, Q.; Lü, Y.; Chen, Y. Synthesis of carbon nanotube array using corona discharge plasma-enhanced chemical vapor deposition. *Chin. Sci. Bull.* **2003**, *48*, 534–537. [CrossRef]

84. Nobuzawa, M.; Sano, N.; Kanki, T. Synthesis of carbon nanotubes forest at a needle electrode by atmospheric pressure corona discharge. In *Asian Pacific Confederation of Chemical Engineers Congress Program and Abstracts*; The Society of Chemical Engineers: Hiroshima, Japan, 2004; p. 66.
85. Bhattacharyya, S.; Staack, D.; Vitol, E.A.; Singhal, R.; Fridman, A.; Friedman, G.; Gogotsi, Y. Localized synthesis of metal nanoparticles using nanoscale corona discharge in aqueous solutions. *Adv. Mater.* **2009**, *21*, 4039–4044. [CrossRef]
86. Jirásek, V.; Lukeš, P.; Kozak, H.; Artemenko, A.; Člupek, M.; Čermák, J.; Rezek, B.; Kromka, A. Filamentation of diamond nanoparticles treated in underwater corona discharge. *RSC Adv.* **2016**, *6*, 2352–2360. [CrossRef]
87. Khataee, A.; Rad, T.S.; Vahid, B.; Khorram, S. Preparation of zeolite nanorods by corona discharge plasma for degradation of phenazopyridine by heterogeneous sono-Fenton-like process. *Ultrason. Sonochem.* **2016**, *33*, 37–46. [CrossRef]
88. Chokradjaroen, C.; Wang, X.; Niu, J.; Fan, T.; Saito, N. Fundamentals of solution plasma for advanced materials synthesis. *Mater. Today Adv.* **2022**, *14*, 100244. [CrossRef]
89. Kim, H.; Watthanaphanit, A.; Saito, N. Simple solution plasma synthesis of hierarchical nanoporous MnO_2 for organic dye removal. *ACS Sustain. Chem. Eng.* **2017**, *5*, 5842–5851. [CrossRef]
90. Kim, H.-M.; Saito, N.; Kim, D.-W. Solution Plasma-Assisted Green Synthesis of MnO_2 Adsorbent and Removal of Cationic Pollutant. *J. Chem.* **2019**, *2019*, 7494292. [CrossRef]
91. Petrović, M.; Jovanović, T.; Rančev, S.; Kovač, J.; Velinov, N.; Najdanović, S.; Kostić, M.; Bojić, A. Plasma modified electrosynthesized cerium oxide catalyst for plasma and photocatalytic degradation of RB 19 dye. *J. Environ. Chem. Eng.* **2022**, *10*, 107931. [CrossRef]
92. Kim, H.; Watthanaphanit, A.; Saito, N. Synthesis of colloidal MnO_2 with a sheet-like structure by one-pot plasma discharge in permanganate aqueous solution. *RSC Adv.* **2016**, *6*, 2826–2834. [CrossRef]
93. Boruah, P.J.; Khanikar, R.R.; Bailung, H. Synthesis and characterization of oxygen vacancy induced narrow bandgap tungsten oxide ($WO_{3-x)}$ nanoparticles by plasma discharge in liquid and its photocatalytic activity. *Plasma Chem. Plasma Process.* **2020**, *40*, 1019–1036. [CrossRef]
94. Zhao, L.; Wang, Y.; Sun, Z.; Wang, A.; Li, X.; Song, C.; Hu, Y. Synthesis of highly dispersed metal sulfide catalysts via low temperature sulfidation in dielectric barrier discharge plasma. *Green Chem.* **2014**, *16*, 2619–2626. [CrossRef]
95. Marino, E.; Huijser, T.; Creyghton, Y.; van der Heijden, A. Synthesis and coating of copper oxide nanoparticles using atmospheric pressure plasmas. *Surf. Coat. Technol.* **2007**, *201*, 9205–9208. [CrossRef]
96. Li, X.; Zhang, J.; Zhou, F.; Zhang, H.; Bai, J.; Wang, Y.; Wang, H. Preparation of N-vacancy-doped g-C_3N_4 with outstanding photocatalytic H_2O_2 production ability by dielectric barrier discharge plasma treatment. *Chin. J. Catal.* **2018**, *39*, 1090–1098. [CrossRef]
97. Guo, Q.; With, P.; Liu, Y.; Gläser, R.; Liu, C.-J. Carbon template removal by dielectric-barrier discharge plasma for the preparation of zirconia. *Catal. Today* **2013**, *211*, 156–161. [CrossRef]
98. Kuai, P.-Y.; Liu, C.-J.; Huo, P.-P. Characterization of CuO-ZnO catalyst prepared by decomposition of carbonates using dielectric-barrier discharge plasma. *Catal. Lett.* **2009**, *129*, 493–498. [CrossRef]
99. Wang, X.; Xu, W.; Liu, N.; Yu, Z.; Li, Y.; Qiu, J. Synthesis of metallic Ni-Co/graphene catalysts with enhanced hydrodesulfurization activity via a low-temperature plasma approach. *Catal. Today* **2015**, *256*, 203–208. [CrossRef]
100. Li, S.; Wang, Z.; Jiang, H.; Zhang, L.; Ren, J.; Zheng, M.; Dong, L.; Sun, L. Plasma-induced highly efficient synthesis of boron doped reduced graphene oxide for supercapacitors. *Chem. Commun.* **2016**, *52*, 10988–10991. [CrossRef] [PubMed]
101. Gao, J.; Zhu, X.; Bian, Z.; Jin, T.; Hu, J.; Liu, H. Paving the way for surface modification in one-dimensional channels of mesoporous materials via plasma treatment. *Microporous Mesoporous Mater.* **2015**, *202*, 16–21. [CrossRef]
102. Zhang, J.; Wang, H.; Zhao, Q.; Di, L.; Zhang, X. Facile synthesis of PdAu/C by cold plasma for efficient dehydrogenation of formic acid. *Int. J. Hydrogen Energy* **2020**, *45*, 9624–9634. [CrossRef]
103. Bharti, B.; Kumar, S.; Lee, H.-N.; Kumar, R. Formation of oxygen vacancies and Ti^{3+} state in TiO_2 thin film and enhanced optical properties by air plasma treatment. *Nat. Sci. Rep.* **2016**, *6*, 32355. [CrossRef]
104. Li, B.; Zhao, Z.; Zhou, Q.; Meng, B.; Meng, X.; Qiu, J. Highly efficient low-temperature plasma-assisted modification of TiO_2 nanosheets with exposed {001} facets for enhanced visible-light photocatalytic activity. *Catal. Today* **2014**, *20*, 14763–14770. [CrossRef]
105. Yu, F.; Wang, C.; Li, Y.; Ma, H.; Wang, R.; Liu, Y.; Suzuki, N.; Terashima, C.; Ohtani, B.; Ochiai, T. Enhanced solar photothermal catalysis over solution plasma activated TiO_2. *Adv. Sci.* **2020**, *7*, 2000204. [CrossRef]
106. Saito, G.; Akiyama, T. Nanomaterial synthesis using plasma generation in liquid. *J. Nanomater.* **2015**, *2015*, 123696. [CrossRef]
107. Shi, L.; Zhou, Y.; Qi, S.; Smith, K.J.; Tan, X.; Yan, J.; Yi, C. Pt catalysts supported on H_2 and O_2 plasma-treated Al_2O_3 for hydrogenation and dehydrogenation of the liquid organic hydrogen carrier pair dibenzyltoluene and perhydrodibenzyltoluene. *ACS Catal.* **2020**, *10*, 10661–10671. [CrossRef]
108. Zhou, R.; Zhou, R.; Alam, D.; Zhang, T.; Li, W.; Xia, Y.; Mai-Prochnow, A.; An, H.; Lovell, E.C.; Masood, H. Plasmacatalytic bubbles using CeO_2 for organic pollutant degradation. *Chem. Eng. J.* **2021**, *403*, 126413. [CrossRef]
109. Liu, Y.; Pan, Y.; Wang, Z.-J.; Kuai, P.; Liu, C.-J. Facile and fast template removal from mesoporous MCM-41 molecular sieve using dielectric-barrier discharge plasma. *Catal. Commun.* **2010**, *11*, 551–554. [CrossRef]
110. Liu, Y.; Wang, Z.; Liu, C.-J. Mechanism of template removal for the synthesis of molecular sieves using dielectric barrier discharge. *Catal. Today* **2015**, *256*, 137–141. [CrossRef]

111. Chirokov, A.; Gutsol, A.; Fridman, A.; Sieber, K.; Grace, J.; Robinson, K. Self-organization of microdischarges in dielectric barrier discharge plasma. *IEEE Trans. Plasma Sci.* **2005**, *33*, 300–301. [CrossRef]
112. Zhang, S.; Li, X.-S.; Zhu, B.; Liu, J.-L.; Zhu, X.; Zhu, A.-M.; Jang, B.W.-L. Atmospheric-pressure O_2 plasma treatment of Au/TiO_2 catalysts for CO oxidation. *Catal. Today* **2015**, *256*, 142–147. [CrossRef]
113. Shi, M.; Luo, G.; Zhu, H.; Zou, R.; Hu, J.; Xu, Y.; Yao, H. Surface modification of fly ash by non-thermal air plasma for elemental mercury removal from coal-fired flue gas. *Environ. Technol.* **2021**, *42*, 306–317. [CrossRef]
114. Gong, Z.; Zhong, W.; He, Z.; Liu, Q.; Chen, H.; Zhou, D.; Zhang, N.; Kang, X.; Chen, Y. Regulating surface oxygen species on copper (I) oxides via plasma treatment for effective reduction of nitrate to ammonia. *Appl. Catal. B Environ.* **2022**, *305*, 121021. [CrossRef]
115. Hájková, P.; Tišler, Z. Atmospheric plasma treated hydrotalcite-type catalyst. *Catal. Lett.* **2017**, *147*, 374–382. [CrossRef]
116. Wu, L.; Cai, Y.; Wang, S.; Li, Z. Doping of nitrogen into biomass-derived porous carbon with large surface area using N_2 non-thermal plasma technique for high-performance supercapacitor. *Int. J. Hydrogen Energy* **2021**, *46*, 2432–2444. [CrossRef]
117. Ding, J.; Sun, X.; Wang, Q.; Li, D.-S.; Li, X.; Li, X.; Chen, L.; Zhang, X.; Tian, X.; Ostrikov, K.K. Plasma synthesis of $Pt/g\text{-}C_3N_4$ photocatalysts with enhanced photocatalytic hydrogen generation. *J. Alloys Compd.* **2021**, *873*, 159871. [CrossRef]
118. Liu, Y.; Zhang, S.; Ma, S.; Sun, X.; Wang, Y.; Liu, F.; Li, Y.; Ma, Y.; Xu, X.; Xue, Y. Electronic Structure Modification of MnO_2 Nanosheet Arrays with Enhanced Water Oxidation Activity and Stability by Nitrogen Plasma. *ACS Appl. Mater. Interfaces* **2024**, *16*, 36498–36508. [CrossRef]
119. Xiao, D.; Ruan, Q.; Bao, D.L.; Luo, Y.; Huang, C.; Tang, S.; Shen, J.; Cheng, C.; Chu, P.K. Effects of ion energy and density on the plasma etching-induced surface area, edge electrical field, and multivacancies in $MoSe_2$ nanosheets for enhancement of the hydrogen evolution reaction. *Small* **2020**, *16*, 2001470. [CrossRef] [PubMed]
120. Feng, L.; Zhang, L.; Zhang, S.; Chen, X.; Li, P.; Gao, Y.; Xie, S.; Zhang, A.; Wang, H. Plasma-assisted controllable doping of nitrogen into MoS_2 nanosheets as efficient nanozymes with enhanced peroxidase-like catalysis activity. *ACS Appl. Mater.* **2020**, *12*, 17547–17556. [CrossRef] [PubMed]
121. Liu, S.; Zhou, J.; Liu, D.; Du, K. Modified Mn/ZSM-5 for Non-Thermal Plasma Mineralization of VOCs and DFT Simulation Using a Novel Y-Type ZSM-5 Model. *Catalysts* **2022**, *12*, 906. [CrossRef]
122. Mohan, H.; Mohandoss, S.; Prakash, A.; Balasubramaniyan, N.; Loganathan, S.; Assadi, A.A.; Khacef, A. Cold plasma assisted synthesis of spinel-$CoFe_2O_4$ nanoparticle with narrow bandgap and high magnetic activity. *Inorg. Chem. Commun.* **2024**, *167*, 112754. [CrossRef]
123. Yi, J.; Wang, P.; Li, F.; Chen, Q.; Lei, L. Structural evolution and catalytic mechanism of the non-thermal plasma modified Pd/Al_2O_3 in C_2H_6 catalytic combustion. *Therm. Sci. Eng. Prog.* **2023**, *46*, 102176. [CrossRef]
124. Zhang, S.; Han, W.; Hu, X.; Sun, H.; Fan, Z.; Shao, T. Supported bimetallic hydrogenation catalysts treated by non-thermal plasmas. *Catal. Today* **2023**, *418*, 114076. [CrossRef]